



12-2014

Design and Model of the Frame for HAGRID (Hybrid Array of Gamma Ray Detectors)

Santiago Munoz

University of Tennessee - Knoxville, smunoz@vols.utk.edu

Recommended Citation

Munoz, Santiago, "Design and Model of the Frame for HAGRID (Hybrid Array of Gamma Ray Detectors)." Master's Thesis, University of Tennessee, 2014.
https://trace.tennessee.edu/utk_gradthes/3163

To the Graduate Council:

I am submitting herewith a thesis written by Santiago Munoz entitled "Design and Model of the Frame for HAGRID (Hybrid Array of Gamma Ray Detectors)." I have examined the final electronic copy of this thesis for form and content and recommend that it be accepted in partial fulfillment of the requirements for the degree of Master of Science, with a major in Physics.

Kate L. Jones, Major Professor

We have read this thesis and recommend its acceptance:

Robert Grzywacz, Marianne Breinig

Accepted for the Council:
Carolyn R. Hodges

Vice Provost and Dean of the Graduate School

(Original signatures are on file with official student records.)

Design and Model of the Frame for HAGRID (Hybrid Array of Gamma Ray Detectors)

A Thesis Presented for the

Master of Science

Degree

The University of Tennessee, Knoxville

Santiago Munoz

December 2014

© by Santiago Munoz, 2014

All Rights Reserved.

I would like to dedicate this paper to my family and friends, for supporting me and helping me along the way, specially Chrisanne, for helping me in graduate school since day one; and finally, my wife Sharon, simple for being, now and forever, my better half

Acknowledgements

I would like to thank Kate Jones for allowed me to work on this project and being so patient with me; Karl Smith, Andrew Ratkiewicz and Steven Pain for helping me with the design, they had a lot of amazing ideas; Every member of the Grzywacz-Jones team.

Abstract

Transfer reactions in inverse kinematics have provided critical information in the study of exotic nuclei. However, transfer reactions with charged particles suffer from poor resolution. The measurement of gamma-rays offers several advantages: they provide not only good resolution in measurements but also other information about the nuclei like lifetimes of unstable states. The combination of these two methods would be the ideal situation to gather information about nuclear structure.

HAGRiD, which stands for The Hybrid Array of Gamma Ray Detectors, is a $\text{LaBr}_3(\text{Ce})$ [lanthanum bromide crystal with a cerium activator] scintillation array to measure gamma rays from transfer reactions and decay experiments. The coupling of HAGRiD with other devices that measure charged particles will permit the combination of both methods.

The evolution and testing of a frame for the mounting of HAGRiD will be presented here. This frame will allow the combination of HAGRiD with other devices to achieve the measurement of gamma-rays and charged particles in coincidence.

Table of Contents

1	Nuclear Physics	1
1.1	Nuclear Structure	1
1.1.1	Nuclear Masses and Binding Energy	1
1.1.2	The shell Model	4
1.1.3	Nuclear Decay	8
1.2	Nuclear Reactions	9
1.2.1	Direct Reactions	11
2	Nuclear Astrophysics	15
2.1	Stellar Nucleosynthesis	15
2.1.1	S-process	18
2.1.2	R-process	18
2.1.3	Why measure Gamma-rays?	18
3	Scintillation Detectors	21
4	HAGRID	26
4.1	Design Concepts	28
4.2	Constraints and Design Criteria	29
4.3	Evolution of the Design	29
4.3.1	Prototype 1	29
4.3.2	Prototype 2	32

4.3.3	Prototype 3	35
4.3.4	Prototype 4	40
5	Conclusion: Final Design	46
	Bibliography	50
	Appendices	53
A	Stress and Strain	54
A.1	Stress	54
A.2	Strain	55
	Vita	58

List of Figures

1.1	Binding energy per nucleon vs mass number. Image modified from [2], p.67.	3
1.2	Discontinuities in the energy of the first electric 2^+ state(a) and S_{2n} (b) for ^{208}Pb and ^{132}Sn . The single-particle states above the magic number N=126(^{208}Pb)(c) and N=82(^{132}Sn)(d).Image modified from [4], figure 1.	4
1.3	Harmonic oscillator and infinite well potentials for the shell structure, with atomic spectroscopy notation to indicate the levels. from [2]	6
1.4	At the left, the potential levels by the Wood-Saxon equation. At the right, same potentials but with the inclusion of the spin orbit. modified from [2]	7
1.5	Representation of Rutherford scattering	12
1.6	Representation of a transfer reaction with a deuteron target in inverse kinematics	14
2.1	P-p chain process	16
2.2	Abundance of elements vs atomic number.	16
2.3	Processes starting ^{56}Fe showing both the s- and r-process. Image modified from [2], pg. 777	17
2.4	Chart of nuclei, showing both the r and s process as well as the magic numbers	19
2.5	Gamma-ray spectra of ^{133}Sn from ($^9Be, ^8Be \rightarrow 2\alpha\gamma$). from [5]	19
2.6	Q-value spectrum for the $^{132}Sn(d,p)^{133}Sn$ reaction. from [4].	20

2.7	854 keV gate on $\gamma - \gamma$ coincidence data from ^{133}Sn . from [5]	20
3.1	Schematic of scintillator and photomultiplier operation. Image modified from [2], p.208 and 212	22
3.2	A BrilanceTM 380 ($LaBr_3(Ce)$) crystal with PMT and base by Saint-Gobain Crystals.	24
3.3	^{232}Th Spectra from $LaBr_3(Ce)$ (upper) and NaI(Tl) (lower). Image modified from [7].	25
4.1	Auto-CAD representation of ORRUBA.[11]	27
4.2	HAGRiD with ORRUBA in the center.	27
4.3	Auto-CAD representation of the $LaBr_3(Ce)$, HAGRiD	28
4.4	Hemispheres design for prototype 1	30
4.5	Details of the handles and rails for Prototype 1	31
4.6	Design concept used to represent pillow blocks TBSP-10	31
4.7	Final design for Prototype 1 in isometric view	32
4.8	Prototype 2 (or Rings) in isometric view	33
4.9	Detail about Prototype 2 (or rings) without HAGRiD	34
4.10	Final design for Prototype 2	35
4.11	Peel design for Prototype 3 showing the new arrangement of Detectors	36
4.12	Prototype 3 in isometric view	37
4.13	Rings supporter (cut) holding the detector	38
4.14	Detail of the rings holding the detector	39
4.15	Prototype 3 (whole) in isometric view	40
4.16	Overview of Prototype 4 without peels	41
4.17	Top part of prototype 4: top rail and security bar	42
4.18	Bottom part of prototype 4: bottom rail and half-ring supporters . .	42
4.19	Detail of the rings holding the detector with O-rings	43
4.20	Peel design of prototype 4 with HAGRiD detectors	44
4.21	Prototype 4 without HAGRiD detectors	45

4.22 Prototype 4 with HAGRiD detectors	45
5.1 The HAGRiD frame with the HAGRiD mount	47
5.2 The TSPB 10 open from Thomson Industries	48
5.3 Detail of assemble between pillow block and the HAGRiD frame . . .	48
5.4 Final design for HAGRiD frame and mount with the GODDESS chamber	49
A.1 The free-body diagram of a body. Image modified from [13], p.49. . .	55
A.2 Diagram of strain. Image modified from [13], p.123.	56
A.3 Stress/strain simulation of the frame in prototype 4.	57

Chapter 1

Nuclear Physics

1.1 Nuclear Structure

1.1.1 Nuclear Masses and Binding Energy

Nuclear masses and binding energy are foundational principles and must be understood before considering nuclear structure and nuclear physics. These two concepts are perhaps the most fundamental ideas in nuclear physics, and are also important to understand how elements are produced in the cosmos.

Being one of the most basic properties of the nucleus, along with half-lives, nuclear masses of stable isotopes are known to a precision of 10^{-11} . The masses of unstable isotopes are more difficult to measure due to the short time that they live and difficulties in production.

Equation 1.1 shows the notation used to represent an isotope, whether stable or unstable:

$$_Z^A X_N \quad (1.1)$$

Z is the atomic number and represents the number of protons in the nucleus. N is the number of neutrons and A is the mass number, which can be defined as the sum

of Z and N. X is the chemical symbol. Sometimes isotopes can be written without the Z and N values, as the Z-value is given by the chemical symbol, X (H nucleus has Z=1, Cl has Z=17 and so on); and one could easily find N using $N = A - Z$.

The nuclear mass of an isotope is defined by the mass of the protons and the neutrons that the isotope has and the binding energy. This definition can be written as:

$$M = ZM_{^1H} + NM_n - B/c^2 \quad (1.2)$$

In this equation M is the atomic mass, $M_{^1H}$ is the mass of the neutral hydrogen atom (which includes the mass of the proton and the mass of the electron), M_n is the mass of the neutron, B is the binding energy, and c is the speed of light. Nuclear binding energy can also be defined as the amount of energy required to separate the nucleus into its constituent nucleons. It is also necessary to consider the separation energies for the last neutron or proton. Equations 1.3 and 1.4 show the definition for neutron and proton separation energies, respectively. Equations 1.3a and 1.4a show the definition in terms of the masses.

$$S_n = [M(A - 1, N - 1) + m_n - M(A, N)]c^2 \quad (1.3a)$$

$$S_n = [B(A, N) - B(A - 1, N - 1)] \quad (1.3b)$$

$$S_{2n} = [B(A, N) - B(A - 2, N - 2)] \quad (1.3c)$$

Equations 1.3b and 1.4b show the definition in terms of the binding energies.

$$S_p = [M(A - 1, Z - 1) + M_H - M(A, N)]c^2 \quad (1.4a)$$

$$S_p = [B(A, Z) - B(A - 1, Z - 1)] \quad (1.4b)$$

Equation 1.3c shows the energy to separate 2 neutrons from a nucleon.

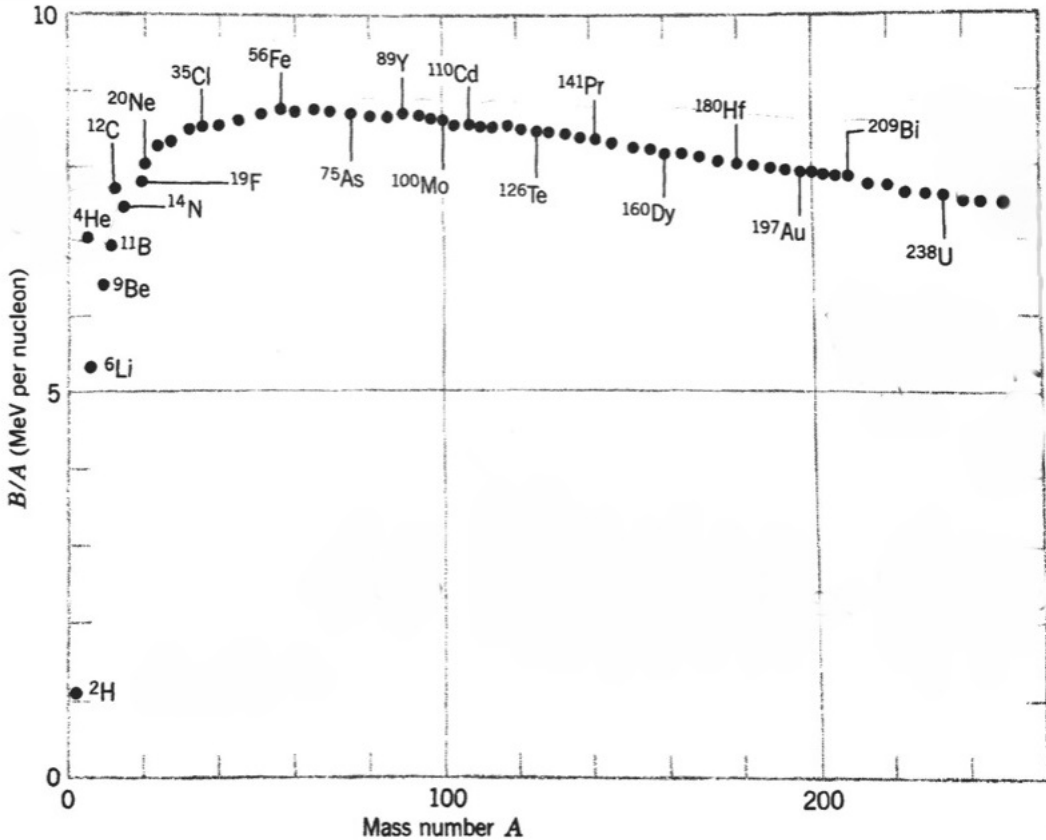


Figure 1.1: Binding energy per nucleon vs mass number. Image modified from [2], p.67.

Binding energy per nucleon can be used as a systematic way of organizing stable isotopes. Figure 1.1 shows this arrangement and it can be seen that the curve peaks around $A \sim 60$, more precisely at $A=62$, with ^{62}Ni (Nickel 62) being the most tightly-bound nucleus. This means that ^{62}Ni requires the most amount of energy, 8.7945×62 MeV, megaelectron volts ($1 \text{ MeV} = 1.602^{-13} \text{ joules}$) to separate into its constituent nucleons . It is often stated that Iron 56 (^{56}Fe) is the isotope with the most binding energy per nucleon, but it is actually the third on the list (with 8.790 MeV), followed by ^{60}Ni (with 8.780 MeV) with Iron 58 in second place (with 8.792 MeV) [3]. These are all close as shown by the flattening of the B/A curve (fig.1.1). Mass energy can be released in two ways: Fusion, which is the combination of two light nuclei to make a heavier nucleus, and fission, which it is the splitting of a heavy nucleus into two

lighter nuclei. These two methods are important for nuclear astrophysics, which will be discussed later on.

1.1.2 The shell Model

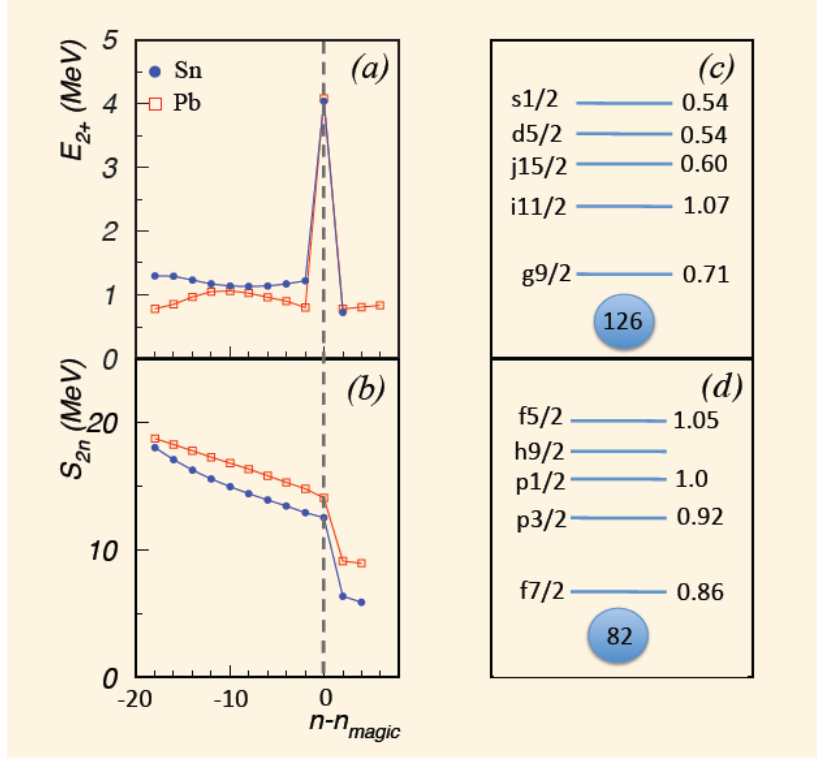


Figure 1.2: Discontinuities in the energy of the first electric 2^+ state(a) and S_{2n} (b) for ^{208}Pb and ^{132}Sn . The single-particle states above the magic number $N=126(^{208}Pb)$ (c) and $N=82(^{132}Sn)$ (d).Image modified from [4], figure 1.

The shell model helps to describe the structure of the nucleus in terms of energy levels. The easiest way to begin to understand the shell model is in comparison to the atomic shell model. The atomic shell model describes the arrangement of electrons in an external Coulomb potential due to the charge of the nucleus by filling levels and following the Pauli principle. The nuclear shell model describes the arrangement of orbitals for neutrons and protons in a nuclear potential. There are some nuclear properties that vary smoothly (see figure 1.2a and b) as the levels are being filled; One of these properties is E_{2+} which is the energy required to allow an isotope to reach

the lowest 2^+ state, a low-lying state in even-even nuclei. Another of these properties is S_{2n} (see equation 1.3c) which is the energy needed to separate 2 neutrons and so removing the effects of pairing, making figures like 1.2b a smooth curve.

There are certain points where there is a sharp discontinuity in the 2 neutron separation energy, S_{2n} , as shown in figure 1.2b, There is also a discontinuity in the energy of the first 2^+ state(a) for ^{208}Pb and ^{132}Sn . These correspond to the filling of a shell. These points are called *magic numbers* (2, 8, 20, 28, 50, 82 for protons and neutrons; and 126 for neutrons) which means that nuclei with these numbers of nucleons are more tightly bound than with an extra nucleon. The discontinuities represent the effects that the next shell is starting fill.

The effect of the magic numbers were discovered before they could be explained, and theories were proposed to try to understand this phenomenon. The first step was to find a nuclear 3D potential like the infinite well or the harmonic oscillator that could be used in calculations to reproduce the measured properties. These potentials were only able to match the first magic numbers (see figure 1.3). Another different potential was proposed, one that would describe the behavior better and mimic the mass distribution of the neutron-neutron interaction. This potential is known as Wood-Saxon potential (see equation 1.5), where $R = 1.25A^{1/3}$ (the nuclear radius), $a = .524\text{fm}$ (the surface thickness) and V_0 is the potential well depth.

$$V(r) = \frac{-V_0}{1 + \exp[(r - R)/a]} \quad (1.5)$$

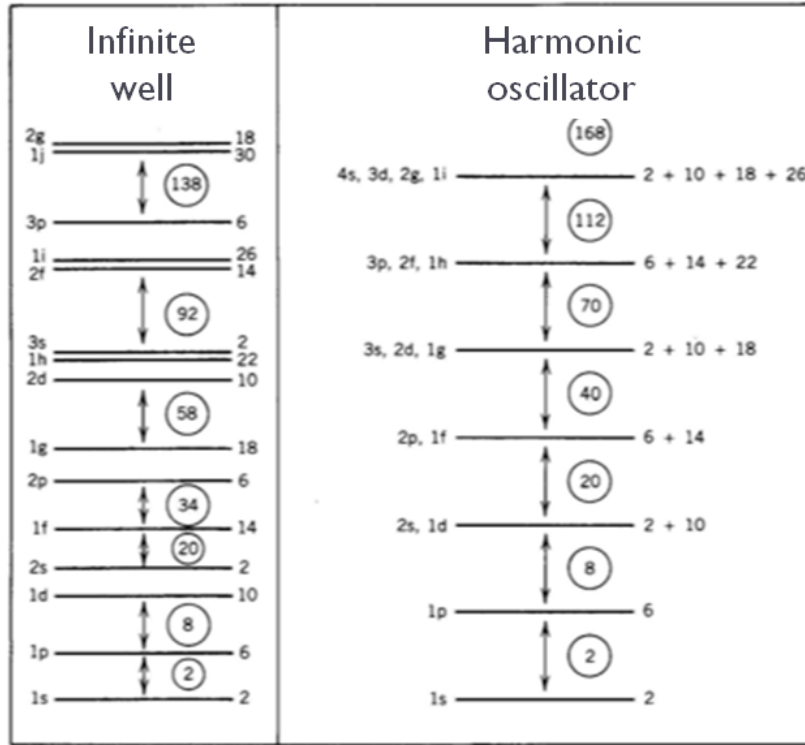


Figure 1.3: Harmonic oscillator and infinite well potentials for the shell structure, with atomic spectroscopy notation to indicate the levels. from [2]

But the Wood-Saxon potential only matched the first magic numbers as shown by the left side of figure 1.4. It was in 1949 that Mayer, Haxel, Suess, and Jensen found the answer to the puzzle by including a *spin-orbit* potential, and so giving the proper separation to the subshells (shown on the right side figure 1.4). The total potential was then as described by equation 1.6 where $V_{ws(r)}$ is the Wood-Saxon potential and $V_{so(r)(l.s)}$ is the spin-orbit potential.

$$V(r) = V_{ws(r)} + V_{so(r)(l.s)} \quad (1.6)$$

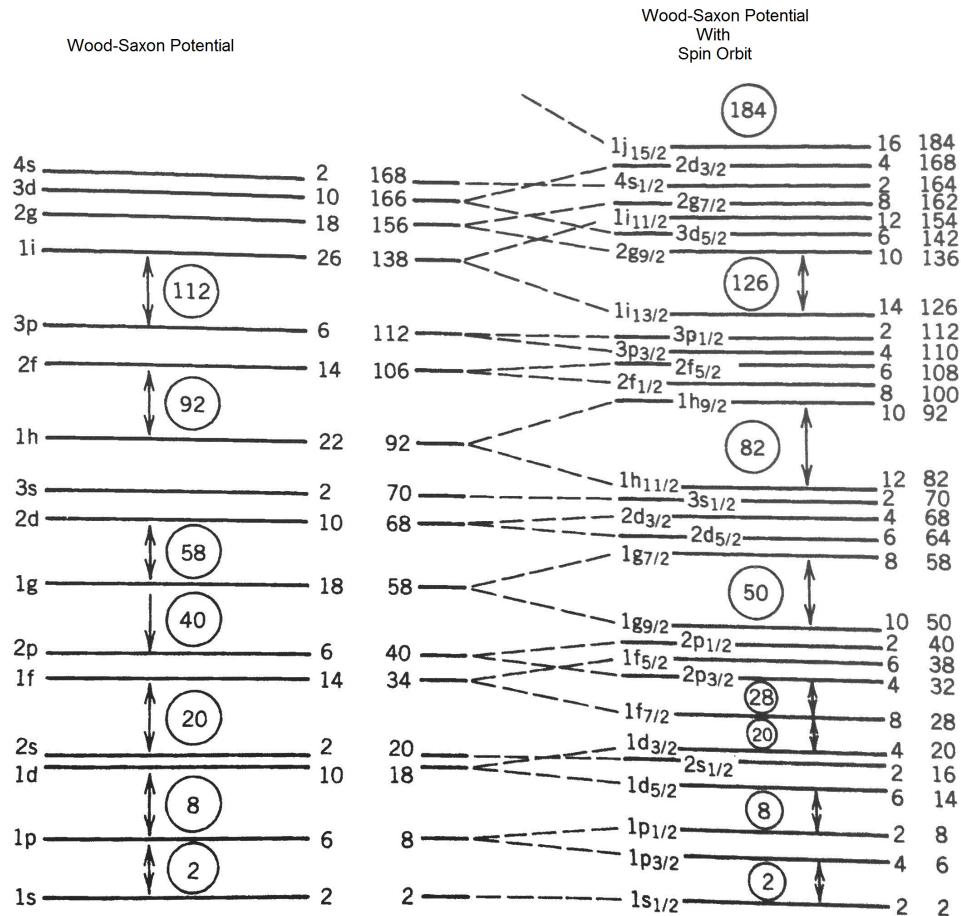
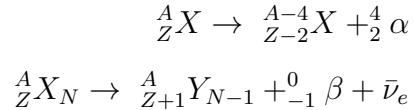


Figure 1.4: At the left, the potential levels by the Wood-Saxon equation. At the right, same potentials but with the inclusion of the spin orbit. modified from [2]

For a given value of l (0 for s, 1 for p, 2 for d and so on as in atomic structure) there are two values of total angular momentum, J since it is defined as $J = l \pm 1/2$. The l.s term (J) is positive for the $+1/2$, and so it is lowered; and negative for $-1/2$, and so it is raised. This system defines the splitting of levels as $2l + 2$, which means the splitting is larger for larger l states. For example the p level has $p_{3/2}$ (a lowered level) and $p_{1/2}$ (a raised level) as shown on the right of figure 1.4. The degeneracy of a state is $J = 2J+1$ which means that there is a space for 2 nucleons in the $p_{1/2}$ and 6 nucleons in $p_{3/2}$ for a total of 8 nucleons, which is a magic number.

1.1.3 Nuclear Decay

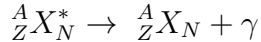
Nuclear decay, also known as radioactive decay, is the process where a nucleus of an unstable atom emits particles or photons and thereby loses energy. Any material is considered radioactive if it emits this kind of radiation energy. Two examples of nuclear decay besides *gamma*(γ) are: *Alpha*(α) which is the process in which an unstable nucleus loses energy by emitting an α particle. The α particle is a nucleus of ${}^4\text{He}$ made up of two neutrons and two protons. Since the original, parent nucleus lost two protons in the process, the daughter nucleus is a different element. In *Beta* (β) which involves an unstable nucleus with an excess of neutrons or protons, the nucleus converts a neutron into a proton and an electron is created and emitted (with an electron anti-neutrino), this is known as β^- ; or the nucleus converts a proton into a neutron and a positron is created and emitted (with an electron neutrino), this is known as β^+ .



Gamma Decay

Gamma decay is the process where an atomic nucleus in an excited state dissipates excess energy in the form of gamma rays (photons or packets of electromagnetic energy of extremely short wavelength) to a lower excited state or the ground state. Since most nuclear reactions can leave the residual nucleus in an excited state, gamma emission commonly follows these reactions, allowing the nucleus to reach the ground state. Gamma emission is usually fast, having half-lives of less than 10^{-9}s . Emissions can sometimes be inhibited, with half-lives of the order of hours. These longer transitions are called isomeric transitions and the long-lived excited states are called isomeric states, isomers, or metastable states [2]. A metastable state is indicated by

a superscript “m”, ($^{58m}_{27}Co$, Cobalt-58m). During a gamma decay process the atomic number (Z) and the neutron number (N) do not change. The following reaction shows a gamma decay in general form, with ${}^A_ZX_N^*$ meaning that the isotope is in an excited state.

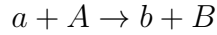


Internal conversion is a process that often competes with γ emission. In this process the nucleus loses its excited state by transferring the energy directly to an atomic electron, which appears as a free electron. Internal conversion is different from β decay in that no change of Z or N occurs [2].

Gamma-ray spectroscopy is one of the main ways to learn about the structure of excited nuclei since gamma-ray energy is easy to detect with high precision and it can be accomplished at high resolution. One of the characteristics of each nuclear species is that they have particular energy levels, so when a gamma ray is emitted, the energy difference of the nuclei can be used to identify particular elements and isotopes.

1.2 Nuclear Reactions

Nuclear reactions are typically performed with a light projectile ion beam ($A \leq 4$) passing a heavy target, resulting in a recoil from the heavy target with a light beam-like particle emerging as well . The goal of a nuclear reaction is to produce a change or transmutation in the nuclei taking part on the process. Rutherford was the first person to correctly interpret a nuclear reaction in 1919. The following notation shows an easy way to understand nuclear reactions:



In this reaction a is the incident light projectile or ion beam; A is the heavy target; b is a resulting, emergent particle; and B is the recoil, target-like nucleus. When a reaction occurs energy can be released, this is known as the reaction Q value (or simply Q value) and it is defined as the initial mass energy $m_0c^2 = (m_a + m_A)c^2$ minus the final mass energy $m_f c^2 = (m_b + m_B)c^2$, (as shown in equation 1.8a). This is equal to sum of the final and initial kinetic energies, T_f and T_0 , respectively (as shown in equations 1.8b). The final kinetic energy T_f is equal to $T_b + T_B$, and the initial kinetic energy T_0 is equal to $T_a + T_A$.

$$Q = (m_0 - m_f)c^2 \quad (1.8a)$$

$$Q = (T_f - T_0) \quad (1.8b)$$

The Q value may be positive ($T_0 < T_f$), negative ($T_0 > T_f$) or zero. When the Q value is positive, the reaction is exothermic. The excess energy is released as kinetic energy of the final products. When the Q value is endothermic or negative, energy has to be applied to the system and some of the initial kinetic energy is converted into nuclear mass or binding energy [2].

There are several types of nuclear reactions and they are classified into direct and compound nucleus reactions. During a direct reaction, if the projectile and target stay in their ground state then the reaction is an elastic scattering and $Q = 0$. If either the projectile or target, or both are left in excited state after the interaction then the reaction is an inelastic scattering and $Q < 0$. The direct reaction is a transfer reaction when one or more nucleons are moved between projectile and target. Knockout is a

high energy direct reaction where one or more nuclei are ejected separately from the interaction. When the direct reaction presents a change in Z (charge) but A stays constant then the interaction is a charge exchange.

If during a reaction the beam and target nuclei stick together the compound nucleus reaction is called fusion. The compound nucleus is often left in a highly excited state that can lead to γ decay or fission. Fusion-evaporation is a compound nucleus reaction where the fusion is followed by particle-evaporation.

Direct reaction including elastic and inelastic scattering, and transfer reactions will be discussed further since HAGRiD is being designed for use in those nuclear reactions.

1.2.1 Direct Reactions

Direct reactions are peripheral processes, in which particles primarily interact at the surface of the target nucleus. They occur on a time scale of the order of 10^{-22} s or approximately the time it takes for a beam particle to pass the target nucleus, while compound nuclear processes take around 10^{-17} s and the nuclei are more central, or closer to each other. In an inelastic scattering the target nucleus, or the projectile, or both take energy from the reaction which allows the nuclei to reach an excited state, which might decay by γ emission. In elastic scattering the target and projectile are in the ground state after the interaction happens. Rutherford scattering, nuclear scattering and transfer reactions are examples of direct reactions.

Rutherford Scattering

Rutherford scattering is a reaction that was used by Geiger and Marsden in early (1911-1913) experiments on the scattering of α particles on a gold target in Rutherford's laboratory at the University of Manchester. Rutherford interpreted the results as the positive charge of an atom being located in a small region at the center of the atom that led to the discovery of the nucleus [2]. Due to the effect of the electrostatic interaction between charged particles, Rutherford scattering is also

known as Coulomb scattering. The electrostatic interaction exists because the nucleus has a distribution of electric charge. Rutherford scattering can be either inelastic or elastic. Figure 1.5 shows the trajectory of a particle undergoing Rutherford scattering. The impact parameter (b) is the distance between the particle's trajectory and a head-on collision.

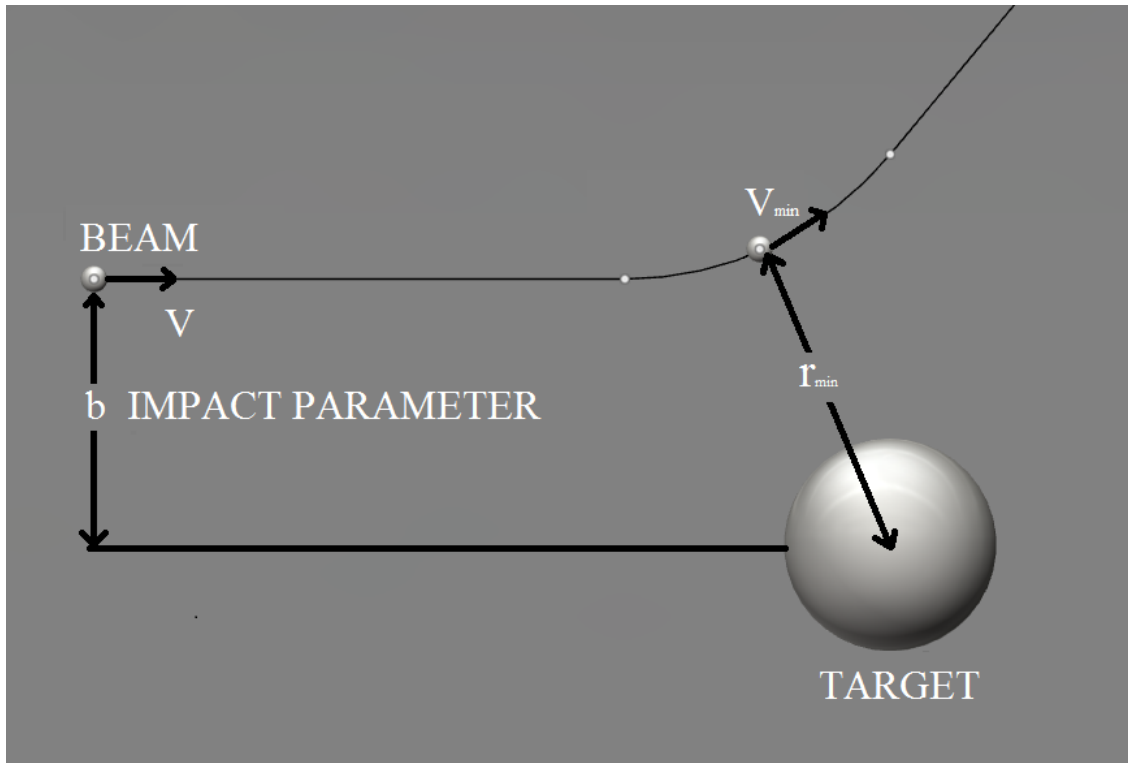


Figure 1.5: Representation of Rutherford scattering

Equation 1.9 defines how the partial cross section changes with angle in Rutherford scattering. In this equation ze is the charge of the projectile and Ze is the charge of the target, $4\pi\epsilon_0$ are the constants from the Coulomb potential energy, T_a is the incident kinetic energy and θ is the scattering angle.

$$\frac{d\sigma}{d\Omega} = \left(\frac{zZe^2}{4\pi\epsilon_0} \right)^2 \left(\frac{1}{4T_a} \right)^2 \left(\frac{1}{\sin \frac{\theta}{2}} \right)^4 \quad (1.9)$$

Nuclear scattering

Nuclear scattering happens when the impact parameter b (see figure 1.5) is small enough so that the projectile and the target can interact through the nuclear (or strong) force. This may not be enough to have pure nuclear scattering, since the Coulomb force will still be present. There are three ways to deal with this interference; the first is to use a neutral particle as projectile. The second is to work at a high energy, so the nuclear force dominates and the projectile can more easily penetrate to feel the nuclear interaction. The third option is to look at angles where Rutherford scattering is very small. There are no equations that can describe the nuclear scattering like equation 1.9 does for Rutherford scattering, since there is not an equation that can describe the strong force exactly. Inelastic nuclear scattering is characterized by having the nucleus or the projectile in an excited state after the interaction dominated by the strong force.

Transfer reactions

Transfer reactions are one way to obtain spectroscopic information from nuclei. Originally these reactions were performed in normal kinematics, with a heavy target and a light ion beam. The exploration of the evolution of nuclear structure requires the study of nuclei away from the valley of stability. This created the need to use inverse kinematics, that is with a light target and a radioactive beam. One-neutron adding reactions like (d,p) (see figure 1.6) allows the acquisition of valuable information from rare ion beams (RIBs), isotopes that would otherwise be hard to make as targets since they would decay before any substantial measure could be achieved. Figure 1.6 shows an example of a transfer reaction where a single neutron is transferred from a deuteron target to a beam projectile. This transfer allows the projectile to reach an excited state to which it would decay to the ground state by gamma decay. Information about the recoil can be gathered by measuring the angles and the energies of the emitted particles, in this case, the proton and γ decays.

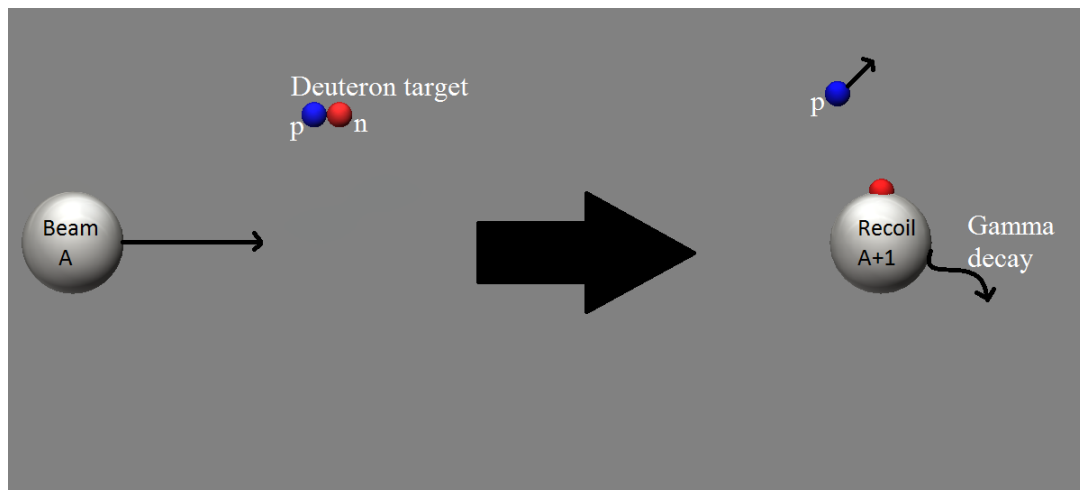


Figure 1.6: Representation of a transfer reaction with a deuteron target in inverse kinematics

Chapter 2

Nuclear Astrophysics

The mysteries of the universe are what drives nuclear physics and astrophysics to perform experiment on earth to explain what happened in space. One of the most important subjects that nuclear astrophysicists study is nuclear fusion inside stars since these events could answer a lot of questions about the universe. Nuclear fusion is the event that fuels stars and stops them from imploding under gravity, at the same time stars provide conditions for fusion which transmutes nuclei thereby producing heavier elements. The heavier the star, the heavier the end products of fusion.

2.1 Stellar Nucleosynthesis

Stellar nucleosynthesis is the process by which elements are created inside stars by combining protons and light nuclei. As stars begin to form from hydrogen and helium gas, gravity begins to pull this gas together and the individual atoms begin to exchange their gravitational potential energy into kinetic energy, and by doing so the temperature also increases. The pressure due to gravity over time becomes large enough to cause the temperature and the density to rise such that protons can overcome the repulsive Coloumb energy and fuse together eventually making alpha particles, through a process called the p-p chain.

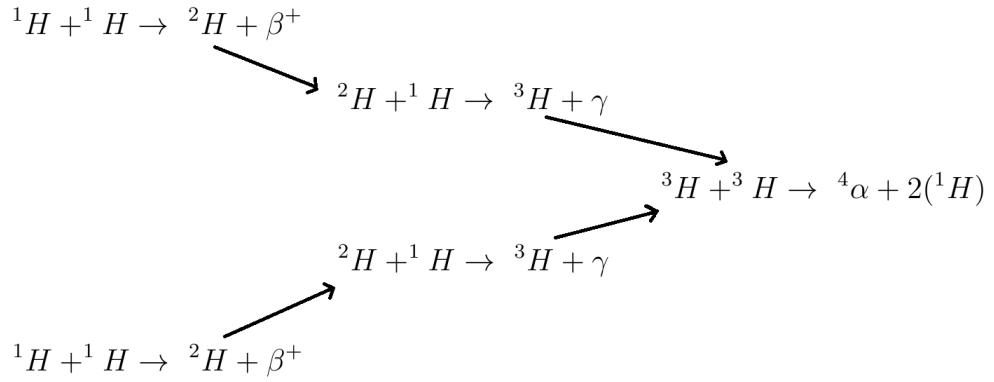


Figure 2.1: P-p chain process

The energy released during this process is what causes stars (like the Sun) to burn. If the star is heavier than the sun, α -particle and nucleon capture reactions also happen as well, allowing the formation of elements up to $A \sim 60$. At this point there is no longer enough energy released in capture reactions and the process is stops. Elements around $A \sim 60$ (${}^{62}\text{Ni}, {}^{56}\text{Fe}$) are the last ones being produced by fusion.

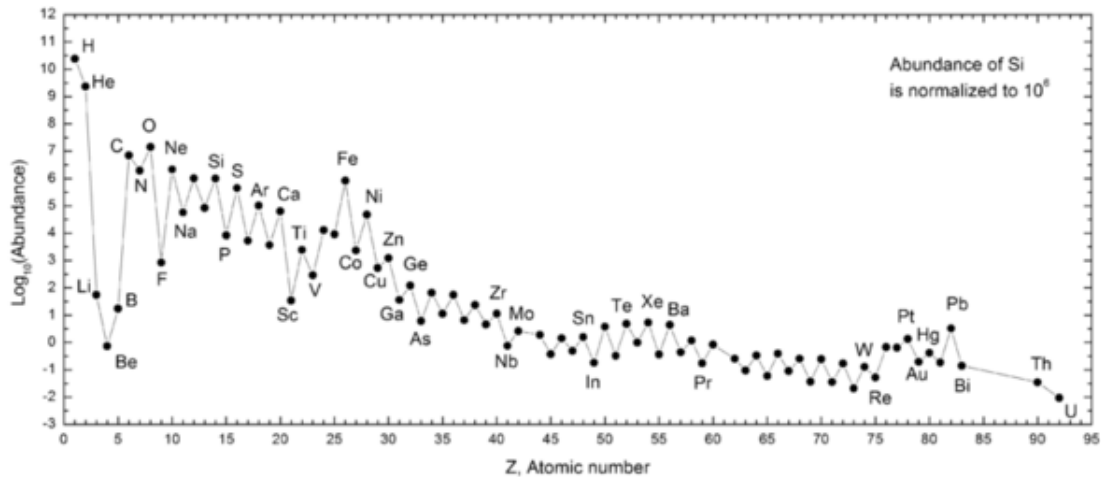
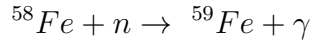
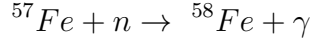
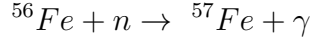


Figure 2.2: Abundance of elements vs atomic number.

Elements beyond $A=60$ are produced by neutron capture reactions, since there is no Coulomb barrier to overcome in this type of reaction. The way neutron capture

processes work is a stable isotope, ^{56}Fe for example, becomes ^{57}Fe by neutron capture, emitting a γ ray and this process keeps happening until an unstable (radioactive) isotope is reached (^{59}Fe), these processes are shown below:



If it does not capture another neutron, ^{59}Fe will β -decay (half-life is 45 days) into ^{59}Co , a stable isotope, and the process of neutron capture will continue for ^{59}Co until an unstable isotope (^{60}Co) decays. These processes continue until an isotope is reached that has a half-life that is shorter than a neutron capture, this isotope β -decays, which takes one unit in the Z-value, and then the process happens again (see figure 2.3). The processes that are responsible for the formation of stable isotopes of nuclei beyond $A = 60$ are known as the s-process and the r-process.

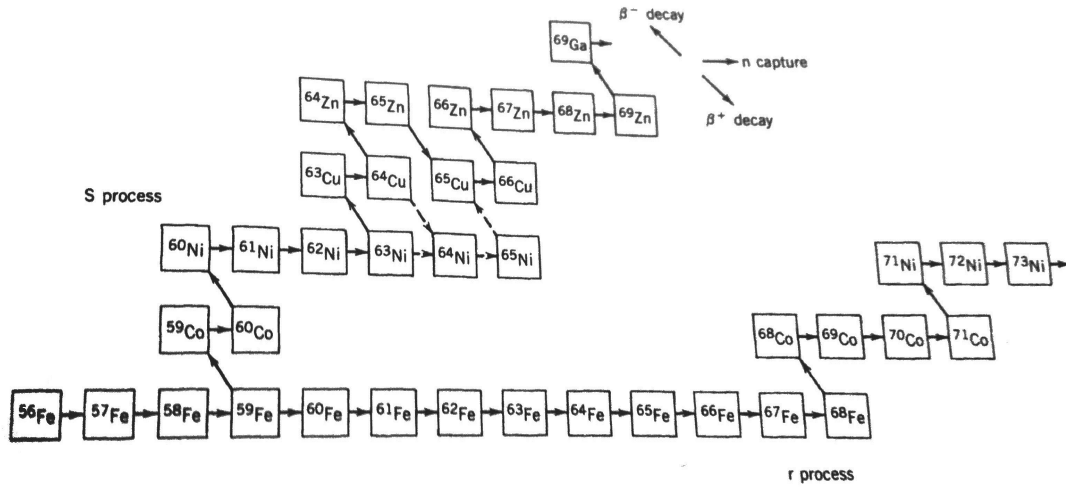


Figure 2.3: Processes starting ^{56}Fe showing both the s- and r-process. Image modified from [2], pg. 777

2.1.1 S-process

The s-process, which stands for the slow-neutron capture process, is one of the major nucleosynthesis processes in the formation of heavy elements ($A>60$). This process occurs in an environment like massive stars, which means that this process moves along the valley of stability (see figure 2.4). The process timescale is in the order of years (neutron capture occurs much slower than in neutron-rich environment).

2.1.2 R-process

The r-process stands for rapid neutron capture process and is responsible for the creation of approximately half of the elements heavier than Iron, as well as the natural group of radioactive isotopes (like bismuth, uranium and thorium) and the most neutron-rich nuclei. The site where this process takes place is unknown but a leading contender is in a core collapse supernovae and it consists of succession of rapid neutron captures. These captures occur much faster than β^- decay for nuclei close to stability so the r-process runs in the neutron-rich region of the nuclear chart (see figure 2.4). Unlike the s-process, most of the r-process nuclei can not be reproduced in an experimental setting. The available data from nuclear structure, like masses and lifetimes, for r-process simulations come from the known properties of accessible nuclei and nuclear model predictions [4].

2.1.3 Why measure Gamma-rays?

There are several advantages for using gamma-rays as a way to discern qualities of an isotope. One of them is that gamma-rays give better resolutions. J.M. Almond *et al.* [5] shows a gamma-ray spectrum (figure 2.5) that presents several interesting energy signatures, When figure 2.5 is compared with data from transfer reaction experiment where only charged particles were detected (figure 2.6) [4] which shows the same energy signatures, it is easy to see the higher resolution presented by figure 2.5.

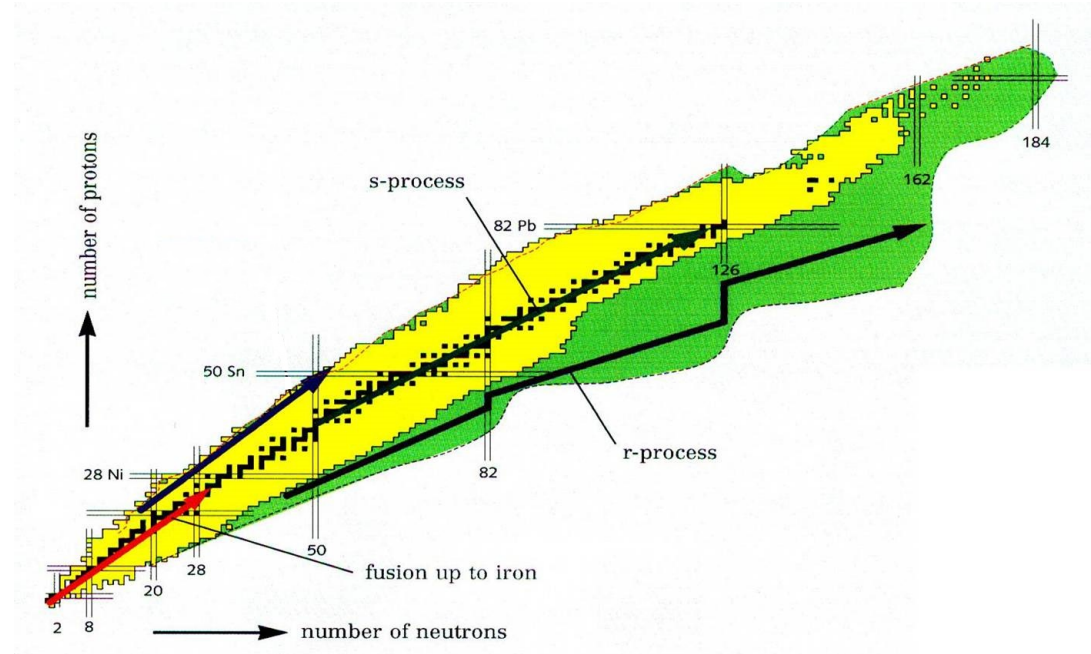


Figure 2.4: Chart of nuclei, showing both the r and s process as well as the magic numbers

Besides the high quality in resolution, gamma-ray spectroscopy allows the collection of more information, for example the lifetimes of states ^{133}Sn and ^{208}Pb were found in the data of figure 2.5 [5] as well as the $\gamma - \gamma$ coincidence used for building level schemes (figure 2.7).

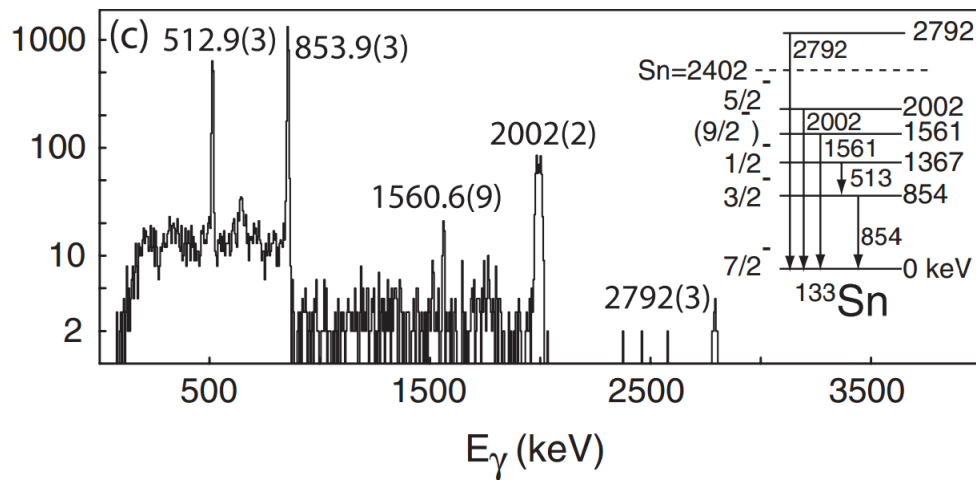


Figure 2.5: Gamma-ray spectra of ^{133}Sn from ($^9Be, ^8Be \rightarrow 2\alpha\gamma$). from [5]

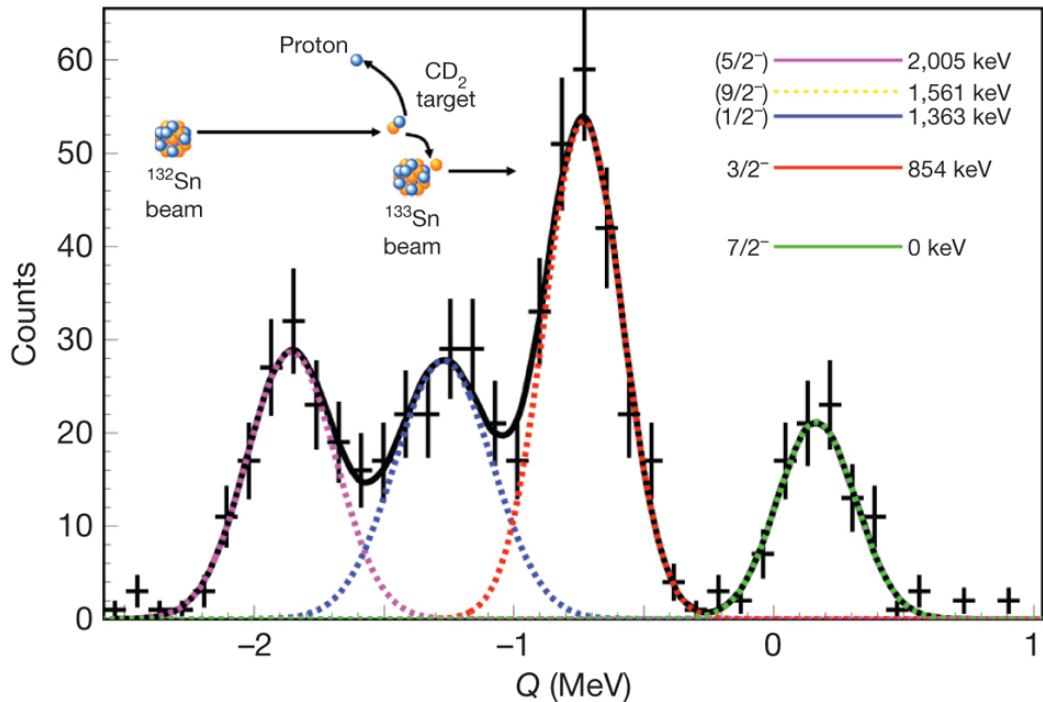


Figure 2.6: Q-value spectrum for the $^{132}\text{Sn}(d,p)^{133}\text{Sn}$ reaction. from [4].

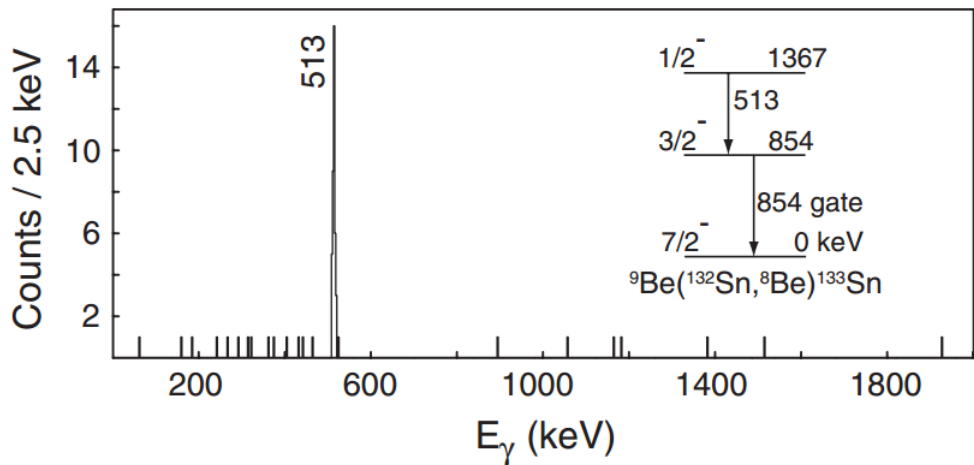


Figure 2.7: 854 keV gate on $\gamma - \gamma$ coincidence data from ^{133}Sn . from [5].

Chapter 3

Scintillation Detectors

A *scintillator* is an organic or inorganic material that has the property of emitting light when hit with ionizing radiation. These type of materials absorb the radiation and then release it back in the form of light. A *scintillation detector* (also known as a scintillation counter) is the combination of a scintillator with a photomultiplier tube (PMT). A PMT consists of a cathode made of photosensitive material followed by an electron collector system, an electron multiplier section and finally an anode from which the final signal can be measured. The function of the PMT is to absorb the light released from the scintillator and turn it into electrons via the p-e effect (see figure 3.1). These electrons are accelerated by an applied voltage, and strike electrodes, releasing secondary electrons that give an electric pulse. Pulses can be used to get meaningful information out of the radiation that hit the scintillation detectors.

The scintillation detector is one of the most widely used particle detections devices in nuclear physics. To better understand a scintillation detector, one needs to know the process that takes place inside of it. first, as shown in figure 3.1, the incident radiation enters the detector and suffers many interactions, which allows the atoms to reach excited states. These excited states rapidly emit (near)visible light, the light strikes the photosensitive surface, releasing at most one photoelectron per photon,

these secondary electrons are then multiplied, accelerated and formed into the output pulse in the photomultiplier (PM) tube [2].

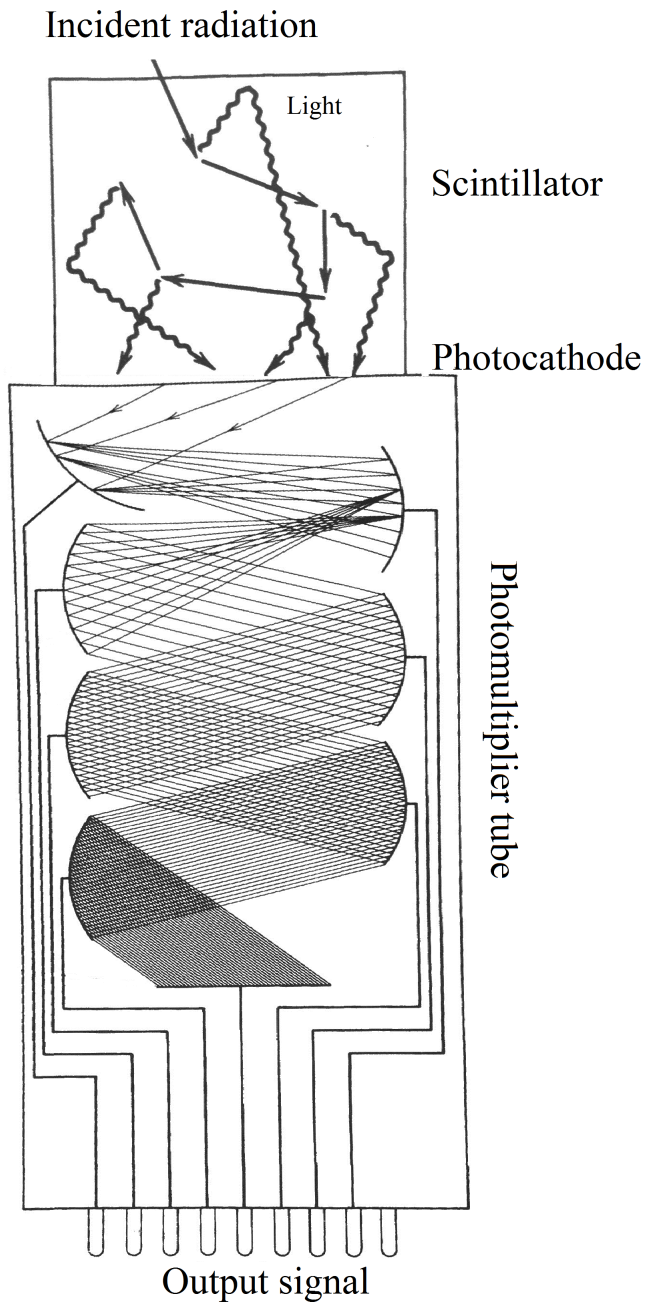


Figure 3.1: Schematic of scintillator and photomultiplier operation. Image modified from [2], p.208 and 212 .

The materials used for a scintillator detectors vary depending on the purpose. The properties that define these materials are light output, efficiency, and energy resolution. The most common materials to be used for scintillators for gamma-ray detection are made from inorganic materials, and are usually an alkali halide salt, such as sodium iodide (NaI) or cesium iodide (CsI). These materials also use an “impurity activator”, the job of these activators is to create special sites in the crystal lattice at which the band gap structure, the energy structure, is modified and thus creates a path which the electron can de-excite through these levels back to the valence band. Thallium and sodium are often used for this purpose, so the way detectors are usually described, for example $\text{NaI}(\text{Tl})$, indicates that it is a sodium iodide crystal with a thallium activator, or as $\text{CsI}(\text{Na})$, which is a cesium iodide crystal with a sodium activator.

Unlike electrons, γ -rays are more efficiently detected by materials with a high atomic number (Z) of protons in the nucleus (called high- Z materials), like gadolinium silicate:Cerium ($\text{GSO}:\text{Ce}$; Gd_2SiO_5) and bismuth germanate, ($\text{Bi}_4\text{Ge}_3\text{O}_{12}$, BGO). The efficiency of gamma-ray detection lies on the photoelectric effect, Compton scattering and pair production. During the photoelectric effect and pair production, the gamma-ray is transformed into a charged particle. During Compton scattering however, the gamma-ray transfers part of its energy to an electron while still remaining a gamma-ray. If this gamma particle escapes, only part of its energy is deposited. In order to create an efficient gamma-ray detector, the material used needs to allow a large cross section for the photoelectric effect and pair production compared to the Compton scattering cross-section [8].

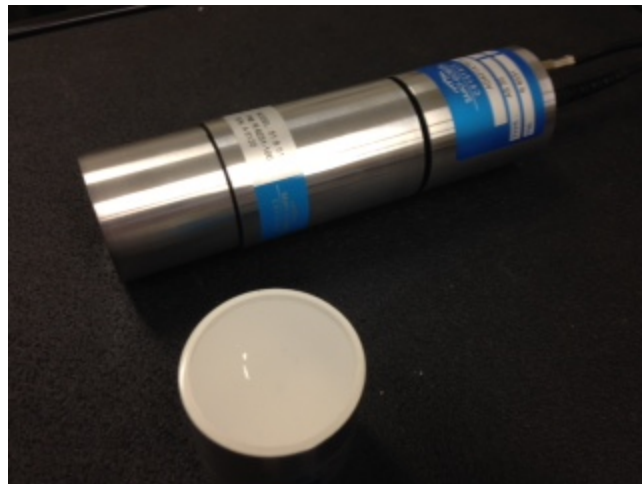


Figure 3.2: A BrilanceTM 380 ($\text{LaBr}_3(\text{Ce})$) crystal with PMT and base by Saint-Gobain Crystals.

$\text{LaBr}_3(\text{Ce})$, which is a lanthanum bromide crystal with a cerium activator, is the inorganic scintillator that is being used for HAGRID (see Ch.5). $\text{LaBr}_3(\text{Ce})$ provides better energy resolution than $\text{NaI}(\text{Tl})$ systems by approximately a factor of 2. The efficiency for $\text{LaBr}_3(\text{Ce})$ is about 1.3 times that of $\text{NaI}(\text{Tl})$ for the same volume and the decay time constant is slower (more than 10%) than the $\text{NaI}(\text{Tl})$ detector decay time. Figure 3.3 shows the difference in resolution between $\text{LaBr}_3(\text{Ce})$ and $\text{NaI}(\text{Tl})$, the spectra are vertically offset to make both visible.

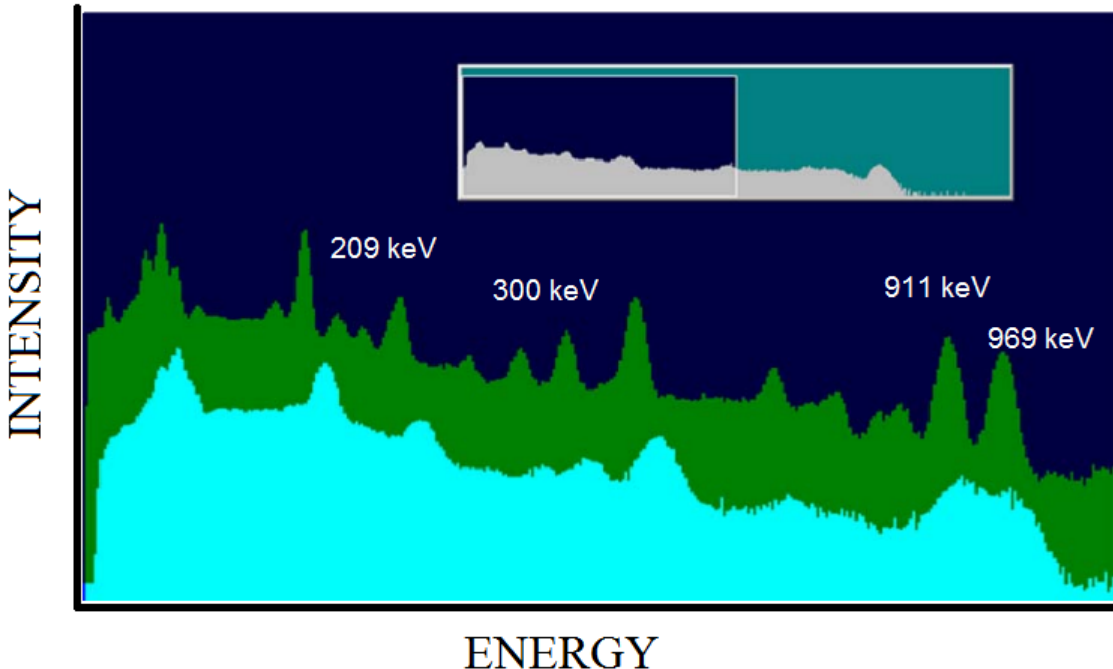


Figure 3.3: ^{232}Th Spectra from $\text{LaBr}_3(\text{Ce})$ (upper) and $\text{NaI}(\text{Tl})$ (lower). Image modified from [7].

Figure 3.3 shows several differences in resolution between $\text{LaBr}_3(\text{Ce})$ and $\text{NaI}(\text{Tl})$. The most noticeable is the poor resolution that $\text{NaI}(\text{Tl})$ presents on the higher energy readings than $\text{LaBr}_3(\text{Ce})$ readings. Several minor gamma-ray signatures (209 and 300 keV) are distinguishable in the $\text{LaBr}_3(\text{Ce})$ spectrum that are not in the $\text{NaI}(\text{Tl})$ spectrum. There are two clear peaks on $\text{LaBr}_3(\text{Ce})$ (around 911-969 keV) that are unresolved in the $\text{NaI}(\text{Tl})$ spectrum.

Chapter 4

HAGRID

Transfer reaction studies and experiments with the detection of charged particles alone have proven to be a successful method for providing information about nuclear structure. However measuring gamma-rays has its advantages, like better resolution in energy. The ideal situation is to perform experiments that would combine these two methods. ORRUBA [§][10] (see figure 4.1) is a positron silicon strip array designed to measure the angle and energy of charged particles, like protons and deuterons. The goal is to use ORRUBA together with HAGRID (see figure 4.2) to use transfer reactions to obtain information about exotic nuclei. This will be done by using ORRUBA to measure the protons (angle and energy) while HAGRID measures the gamma-rays of the excited recoil nucleus.

The Hybrid Array of Gamma Ray Detectors (HAGRID) (see figure 4.3) is a detector designed for use in both transfer reaction and decay experiments. HAGRID will be coupled with ORRUBA and JENSA [‡] for transfer reactions and decay experiments with VANDLE ^{*} and MTAS[†]. HAGRID will also be paired up with other devices like the S800 spectrometer which measures the recoil from transfer reactions.

[§]Oak Ridge Rutgers University Barrel Array

[‡]Jet Experiments in Nuclear Structure and Astrophysics

^{*}Versatile Array of Neutron Detectors at Low Energy

[†]Modular Total Absorption Spectrometer

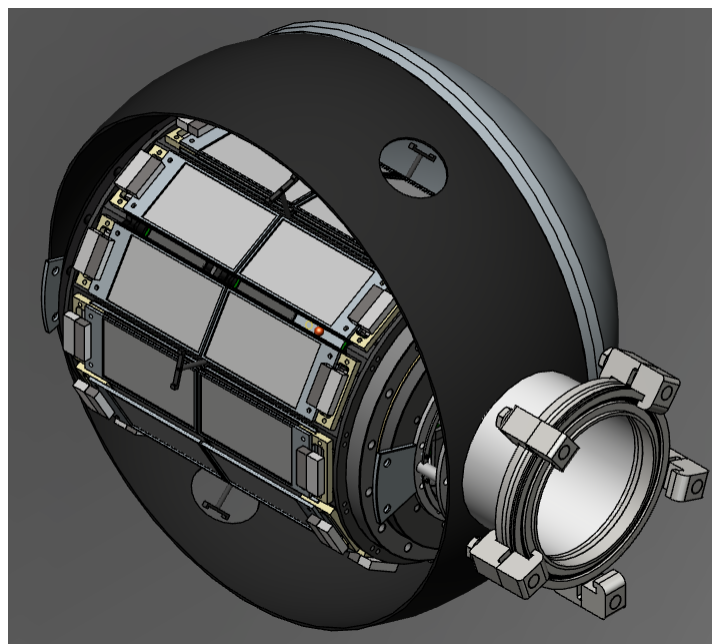


Figure 4.1: Auto-CAD representation of ORRUBA.[11]

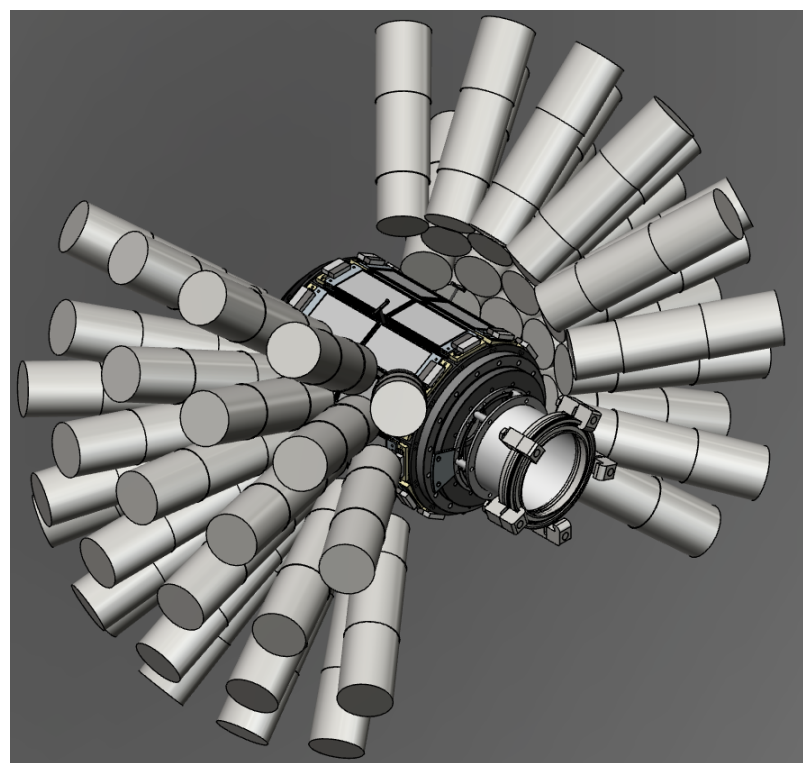


Figure 4.2: HAGRiD with ORRUBA in the center.

The goal of the project is to design a frame for HAGRiD to couple with ORRUBA. Below is a description of the evolution of the frame for mounting the array of approximately 54 $LaBr_3$ scintillators around ORRUBA as would be used to obtain better resolution in a transfer reaction experiment with a possible expansion.

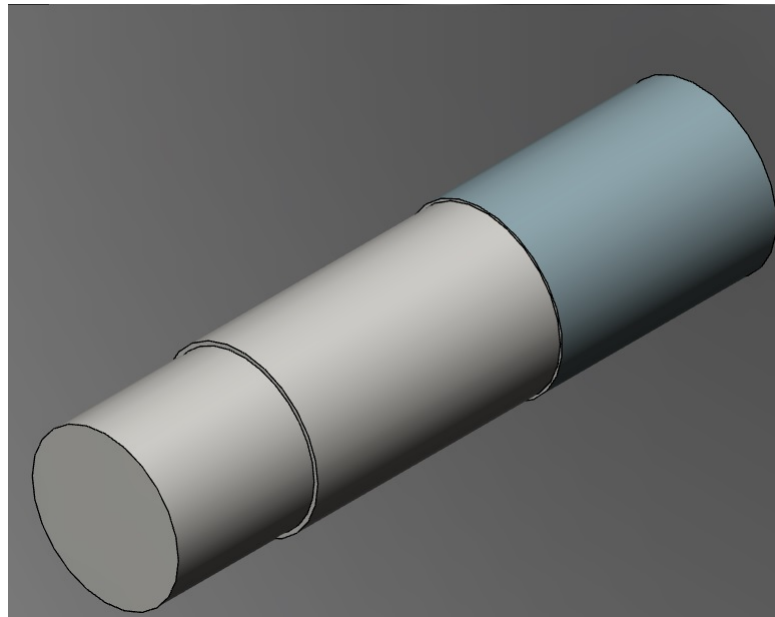


Figure 4.3: Auto-CAD representation of the $LaBr_3(Ce)$, HAGRiD

4.1 Design Concepts

As with any design project, as the original design criteria for the frame were refined the design became more complex. Features were added that allowed the frame to be more versatile, allowing additional sensors to be incorporated as the project develops. Auto-CAD Inventor Fusion 2013 R® was used for the main design work. Later on, Auto-CAD Inventor Professional 2014® was used to finish some details of the final design, and to perform the Stress/Strain tests required.

4.2 Constraints and Design Criteria

There were several challenges present while designing the frame. The frame needed to have a balance between versatility of the mount with portability since the frame will be used in several facilities. One of the biggest constraints for a frame such as this is containment size in order to retain versatility of application in different facilities, since the goal is for the frame to be used in any space possible. Physical constraints were also a problem. Early versions consisted of two hemispheres that keep the detectors together in position. However, the hemisphere shells presented mechanical complications. There were also several criteria that the frame needed to fulfill in order to be useful. All the detectors need to be pointed at the center of ORRUBA, since HAGRiD will be paired up with this detector. All the detectors need to be close together for a complete coverage of angles as possible. All of these need to be done while still allowing the frame to be easy to operate and the target chamber inside to be vacuum sealed. Appendix A shows two important constraints that are always present in every design: stress and strain.

4.3 Evolution of the Design

4.3.1 Prototype 1

The initial concept was to mount the individual LaBr₃ crystals, with attached photomultiplier tubes, in holes in two hemispherical shells as shown in figure 4.4. This design ensures that all the detectors are mounted at the same radius and point at the interaction point on the target. Two rings were used to hold each detector in contact with the hemispherical shell, one outside the shell and one inside, using pressure to hold the detectors in place. The concept of the supporting rings was worked on in further prototypes.

The positions of the detectors in this design are well defined. However, this also results in fixed positions for the detectors, so the measurement angles can not be

changed, and the fixed sizes meant a reduction in flexibility for incorporating other detectors into the array. As mentioned in section 4.2, one of the biggest issues with this design was the difficulty of actually making the hemispherical shells.

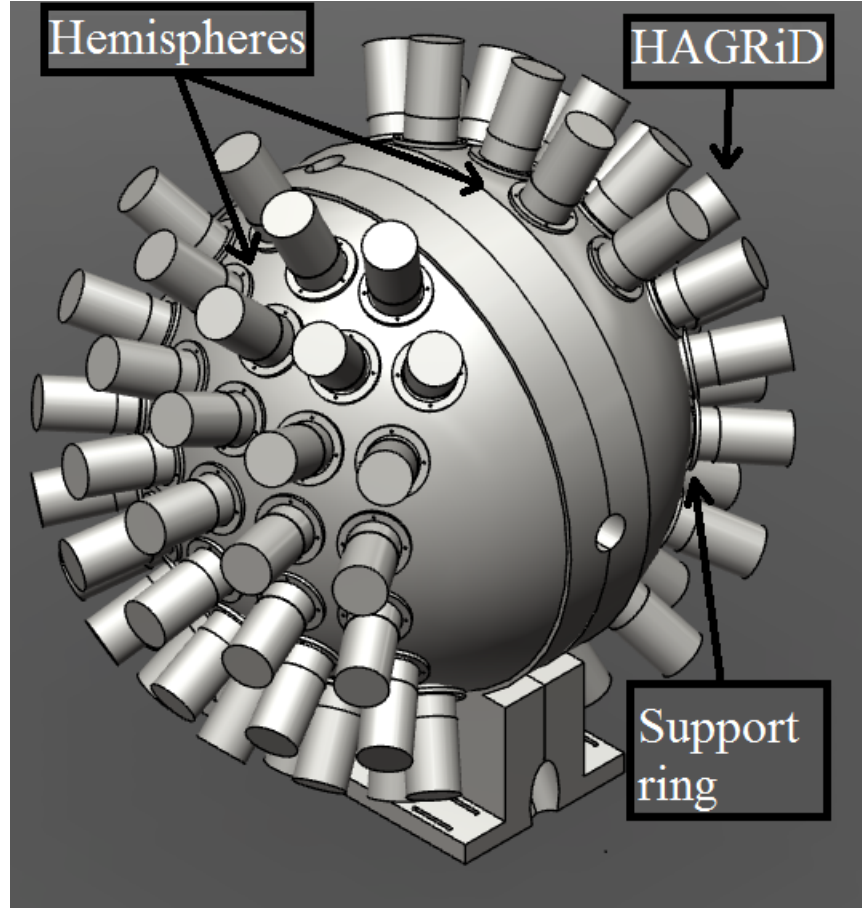


Figure 4.4: Hemispheres design for prototype 1

Handlebars were incorporated into the design to be attached to the shells allowing ease of opening and closing without putting pressure on the detectors (see figure 4.5). Figure 4.5 also shows rails and a base, so the frame could easily move and the hemispheres could be separated. Pillow Blocks (TSPB) from Thomson Industries (see figure 4.6), were used to allow the frame to connect to the rails and base and move freely.

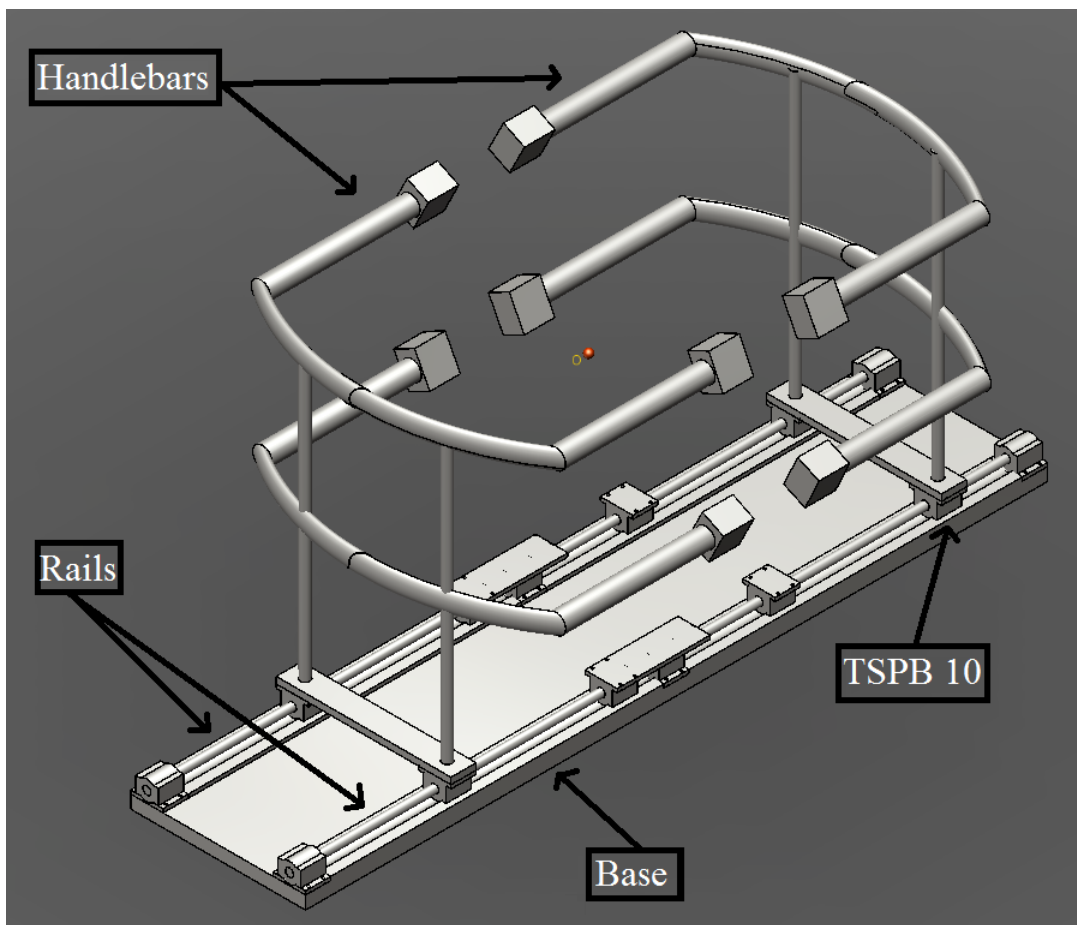


Figure 4.5: Details of the handles and rails for Prototype 1

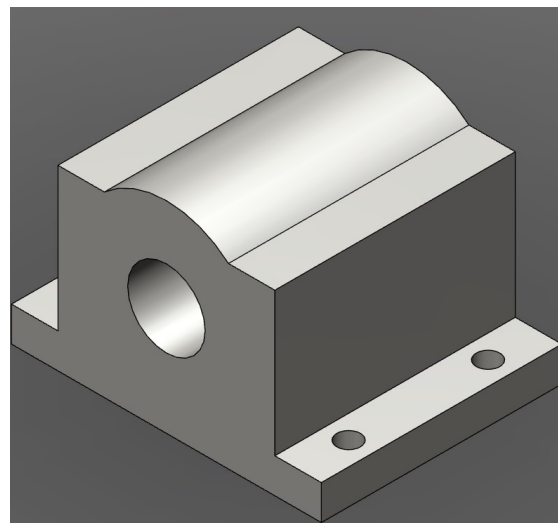


Figure 4.6: Design concept used to represent pillow blocks TBSP-10

As stated before, prototype 1 was ultimately discarded because of the complications presented by the manufacturing of the hemispheres, but all of the other ideas (handle bars, rails base and pillow blocks) were implemented in later designs, with some changes.

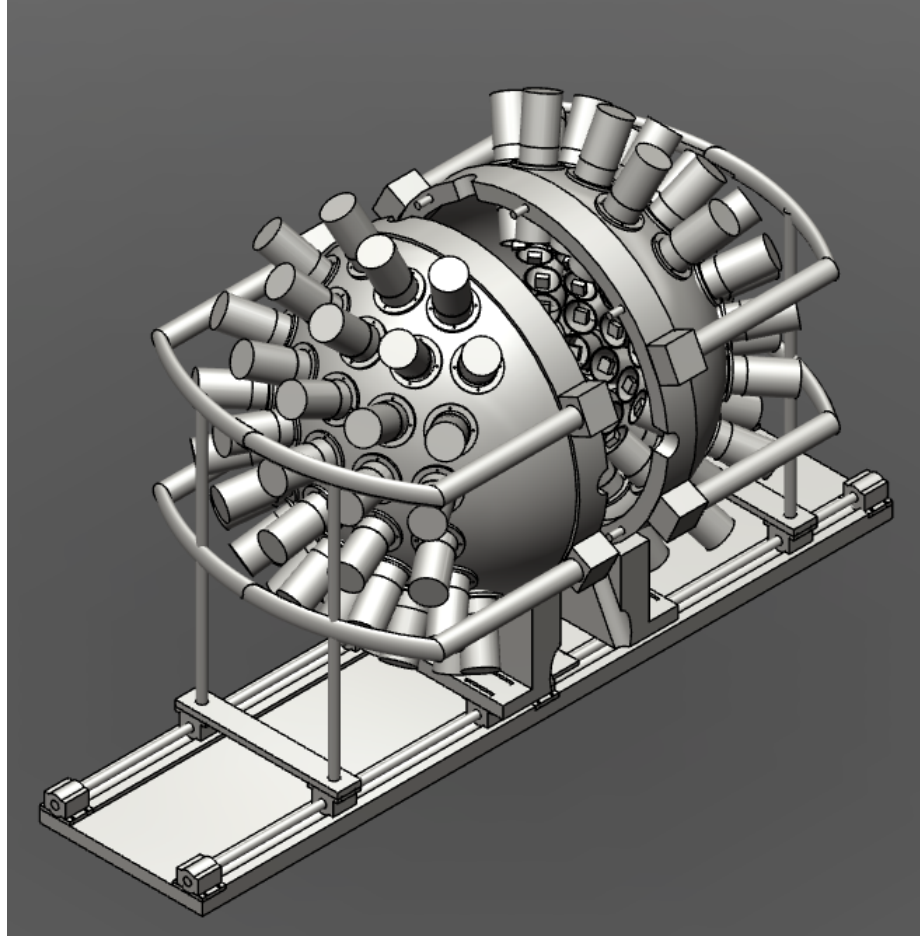


Figure 4.7: Final design for Prototype 1 in isometric view

4.3.2 Prototype 2

This design focused on the hemispheres' inflexibility and manufacturing issues, so half-rings were used instead. These ribs were attached at the top and bottom. These half-rings were meant to allow a wider range of angles per detector by being able to rotate, but that was never implemented in this design.(see figure 4.8)

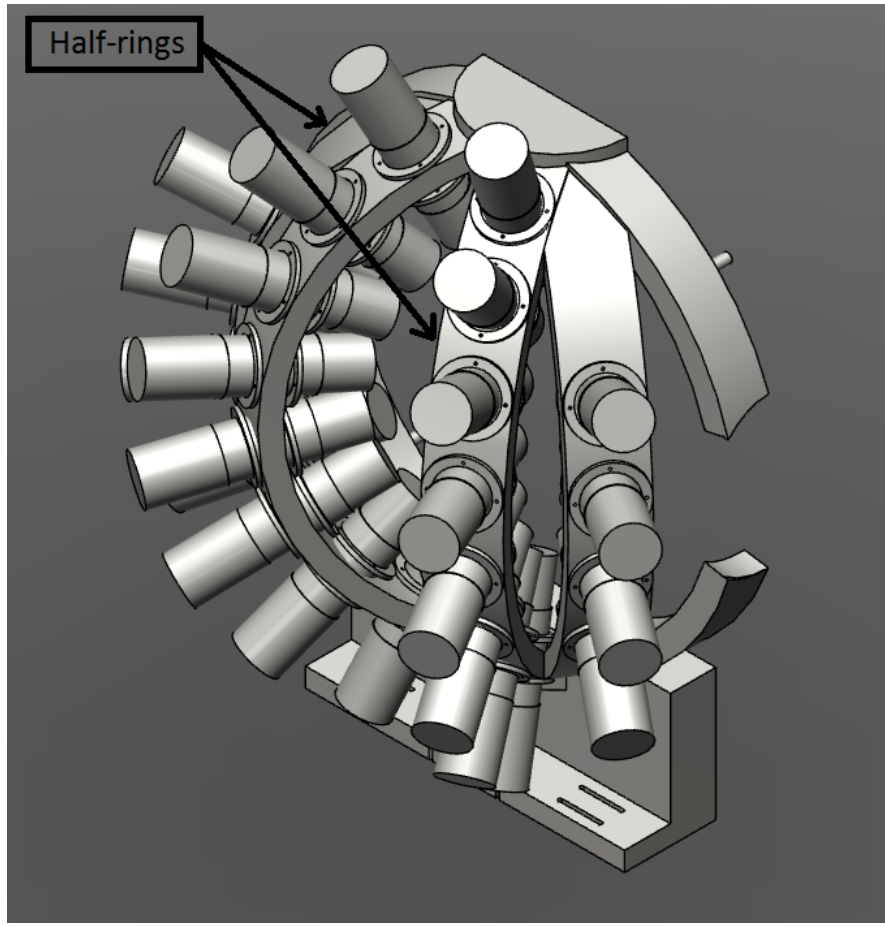


Figure 4.8: Prototype 2 (or Rings) in isometric view

The handle bars were used again but they were changed to a vertical position to allow easy access to each detector as shown in figure 4.9. An early concept of the security bars were used. Here they are meant to be part of the handle bars. These security bars had their own base and they, along with the handle bars, were meant to separate from the frame. Pillow Blocks (TBSP10) were still used in this prototype, as well as the rails and the base from prototype 1 (see figure 4.10)

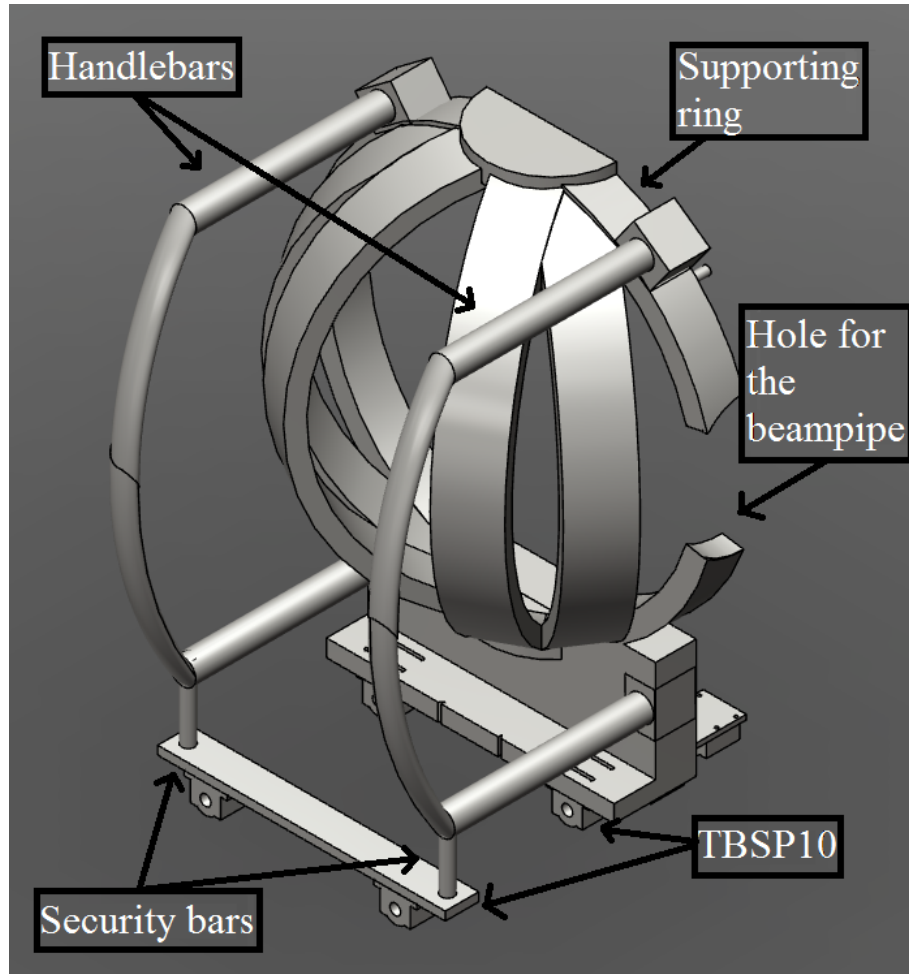


Figure 4.9: Detail about Prototype 2 (or rings) without HAGRiD

Prototype 2 was not chosen due to fact that the integrity of the supporting rings was compromised since they had a hole to let the beam pipe out (see figure 4.9). The idea of being able to change the angle of the detectors was better in terms of data collection and practicality, and was retained in the next design stages.

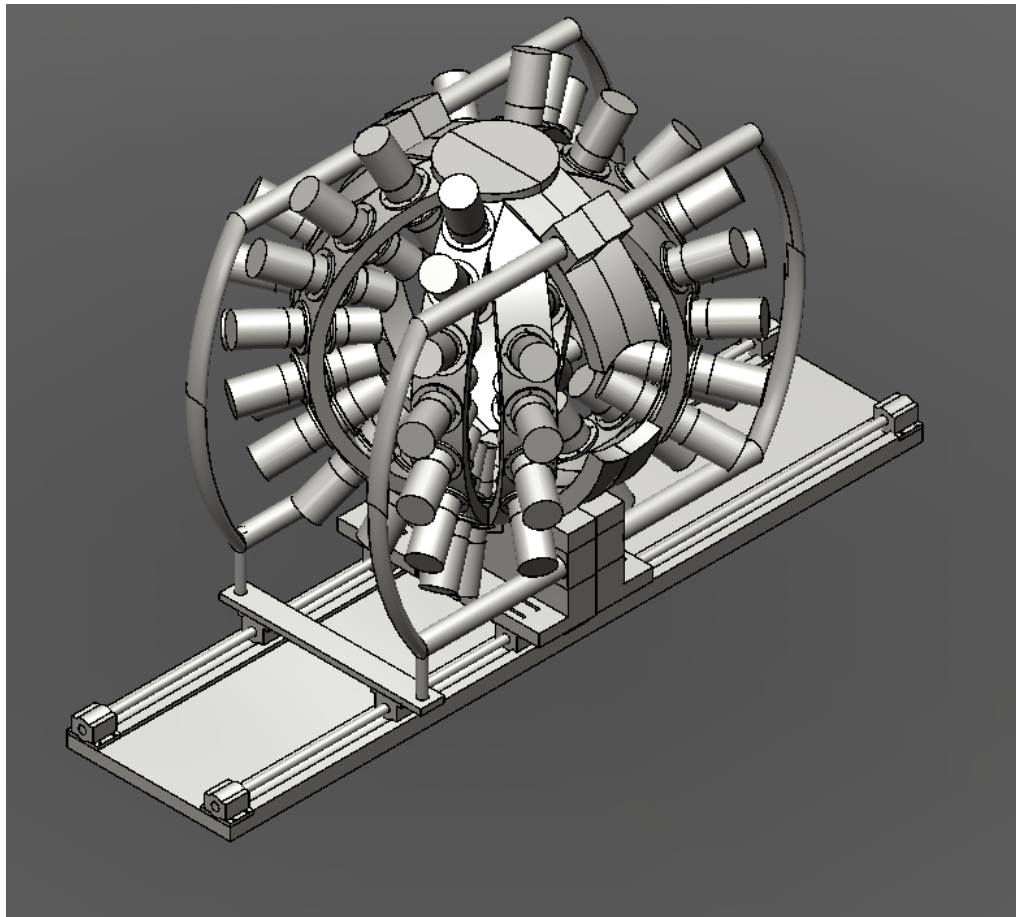


Figure 4.10: Final design for Prototype 2

4.3.3 Prototype 3

This design was a step further in the direction that was taken in prototype 2. Peels (see figure 4.11) were used instead of half-rings. The peels are narrow at top and bottom and wider in the center, so putting the detectors in a straight line would not be really effective. The methods presented by D.W. Clare and D.L. Kepert on “The Optimal Packing of Circles on a Sphere” [12] were used to solve the peels’ limited space and obtain the maximum number of detectors per peel.

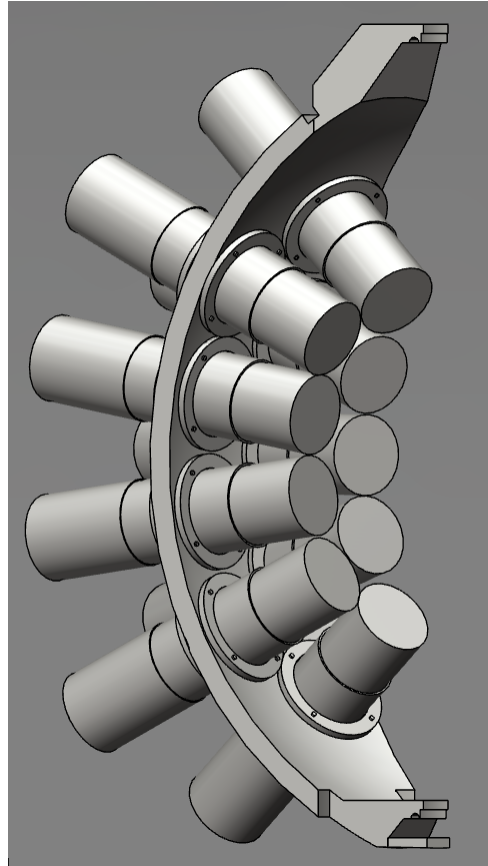


Figure 4.11: Peel design for Prototype 3 showing the new arrangement of Detectors

Rails were used at the top and bottom of the main structural ring (see figure 4.12), and the peels were modified so they can hook on these rails. These modifications allowed the peels to be rotated, giving them wider flexibility in the range of angles covered. A bar was implemented as a security measure, so the peels would not fall back in case they are not completely hooked to the rails. The base of the frame was made longer to give more stability and a rib below the base of the structural ring was also implemented for the same purpose. The handle bars were also connected to the base via two independent short bars, these bars gave more stability and helped distribute the weight of the whole upper structure. The addition of the bolts, screws, and nuts in the actual design give this prototype a more realistic sense. The whole frame was made for easy construction, transportation and access.

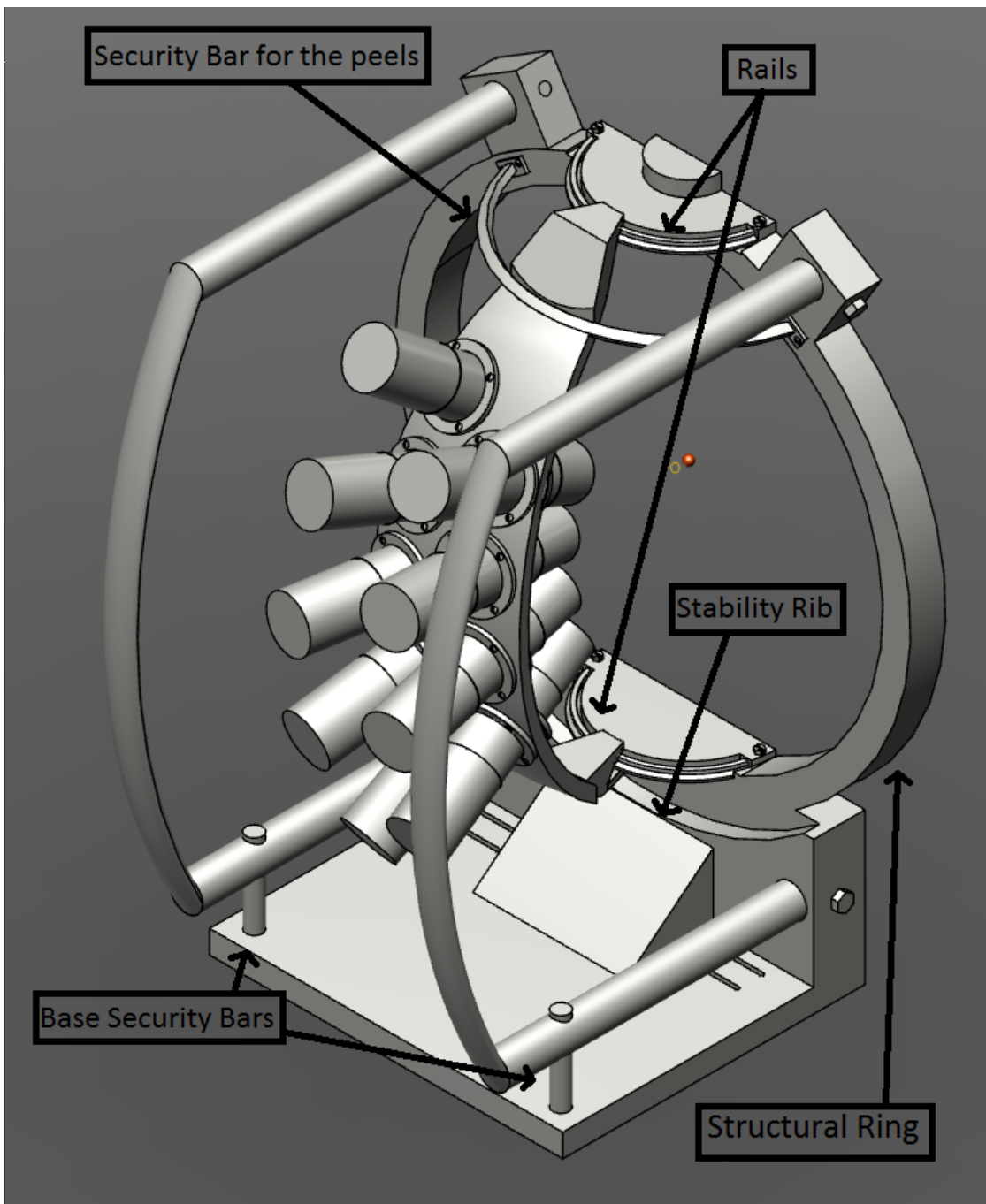


Figure 4.12: Prototype 3 in isometric view

The question of how the detectors are held in the frame was perhaps one of the biggest challenges in the design of the HAGRiD frame, if not the biggest. Figure 4.13 shows the proposed solution. The HAGRiD detectors will be held in place

by two support rings (per detector), these rings will have a curvature (as shown in figures 4.13 and 4.14). The screws and nuts will create a force on the support rings when tightened this creates pressure on the detector due to the curvature on the ring-supporters, as detailed in figure 4.14. The only problem with this idea is that the pressure exerted by the support rings might harm the detector, so this concept was improved in prototype 4.

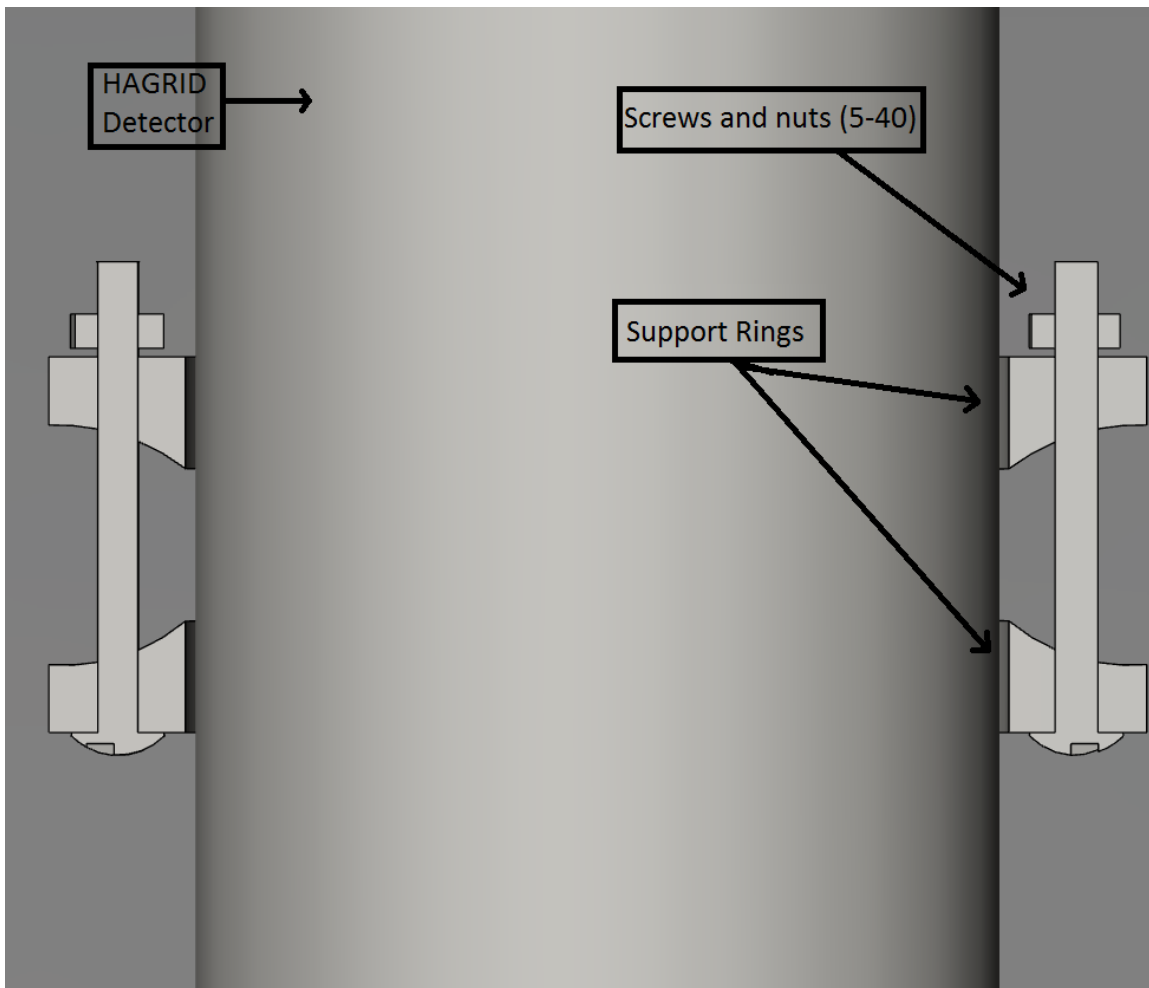


Figure 4.13: Rings supporter (cut) holding the detector

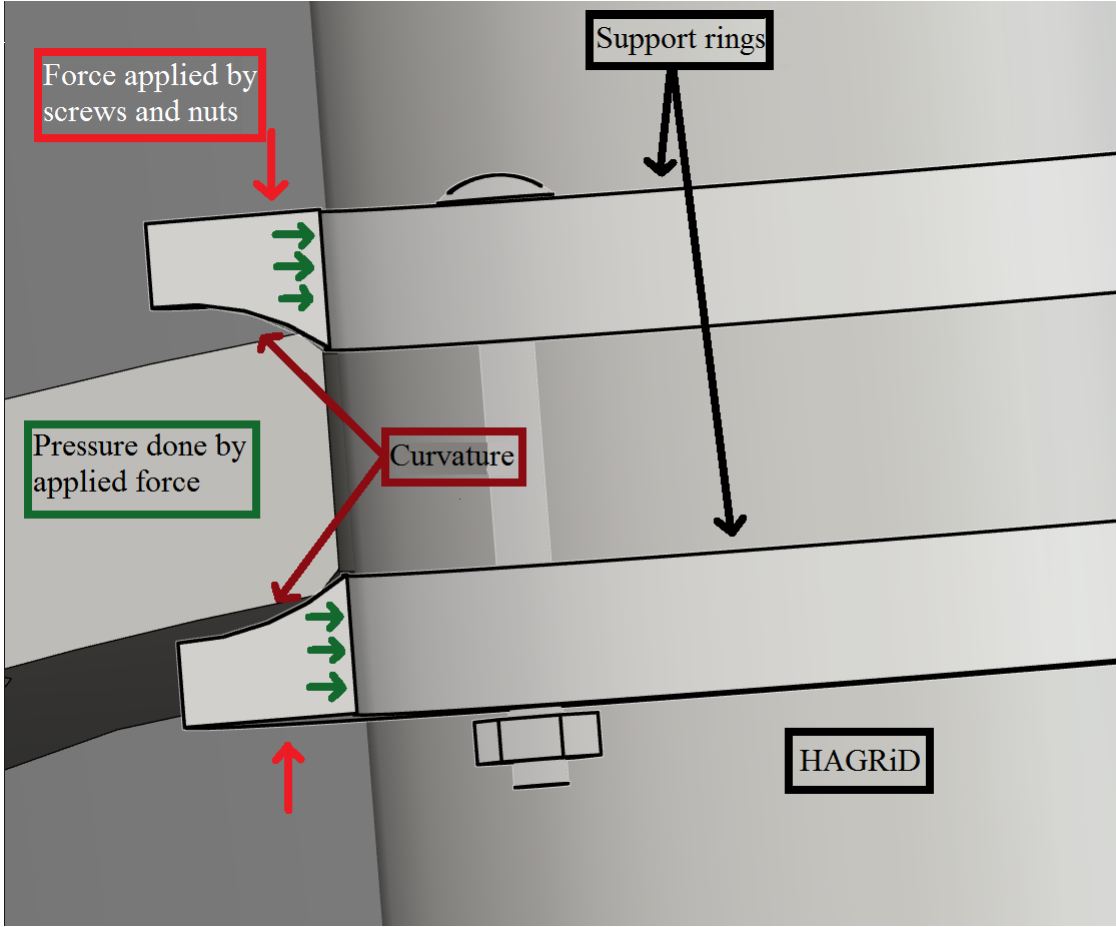


Figure 4.14: Detail of the rings holding the detector

Figure 4.15 shows the complete design of prototype 3 without the detectors, with both sides connected and 4 peels per side. A cap was designed as a way to secure the connection between the two halves of the frame. Ultimately this design, prototype 3, was not selected for two reasons: first, the still limited angle range of the peels and second, the structural rings needed to be cut so the beam line could go through the frame. This would have compromised the integrity of the whole frame.

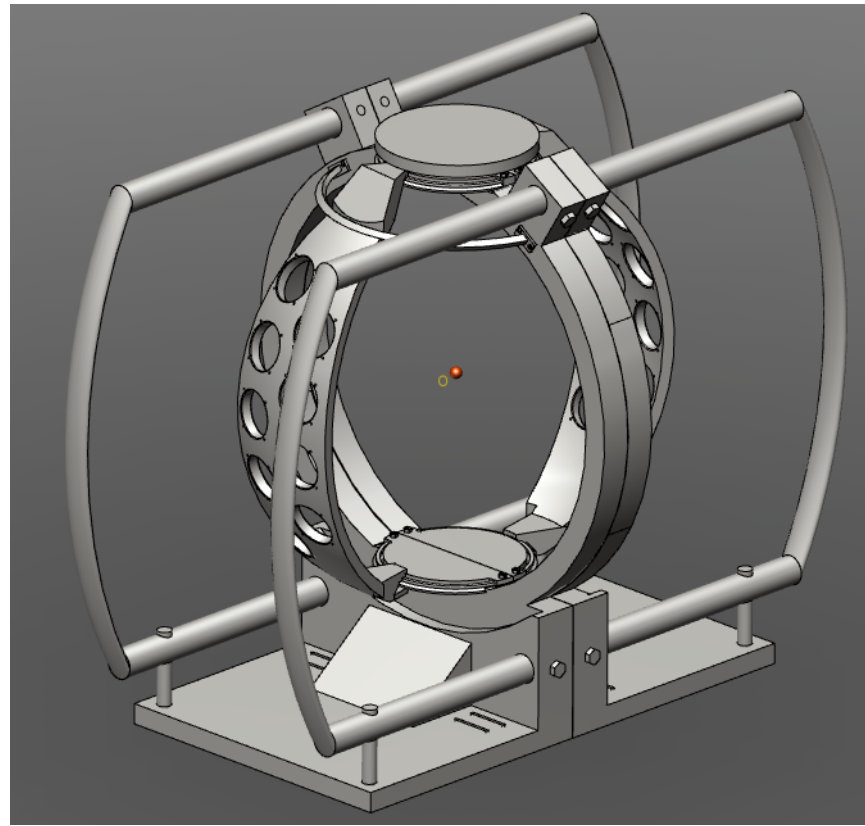


Figure 4.15: Prototype 3 (whole) in isometric view

4.3.4 Prototype 4

The goal for the design in Prototype 4 was to improve on the flaws of prototype 3, however a new approach was taken on the design. The first thing that needed to be improved in prototype 3 was the limited angle range of the peels so the structural ring was totally discarded. The main structure was divided in two (top and bottom) and joined together by two half-rings (see figure 4.16) which support the entire structure. The idea of the handle bars was used again, but this time it helped to connect both parts as well.

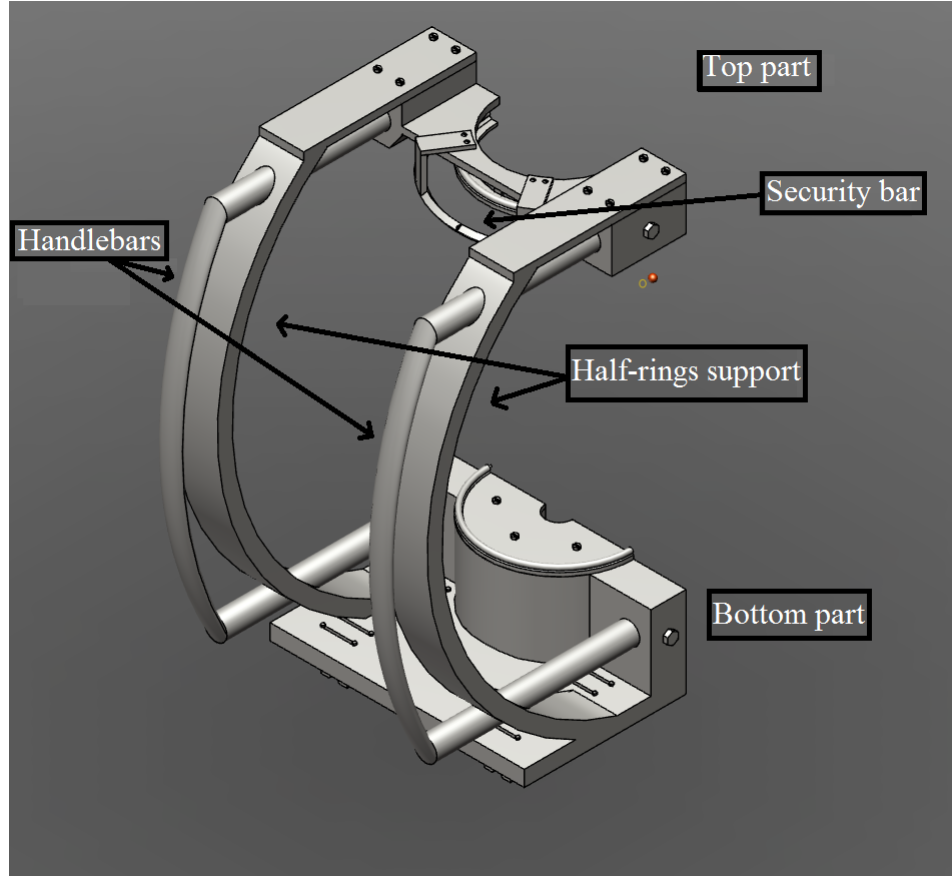


Figure 4.16: Overview of Prototype 4 without peels

The idea of the rails was also improved. The top rail was modified so it would allow the peels to be positioned at any angle in the range from 0° to 180° (so when both halves of the frame are together, it would be 0° to 360°). The security bar was included as a security measure, but it also provides a way to measure the angles. As shown in figures 4.16 and 4.17, the top rail and the security bar are the top part of the frame, along with the piece that connects them to the handle bars and the half-ring support.

Although some modifications were made to fit with the other changes of the frame, most of the frame in prototype 3 became the bottom part in prototype 4. Figure 4.18 shows the addition of a center semi-hole that will allow a mount for the target chamber as well as, four sets of holes that were added to the base to allow the frame to be

connected to other mounts; The stability rib was modified as well, to fit the new bottom rail.

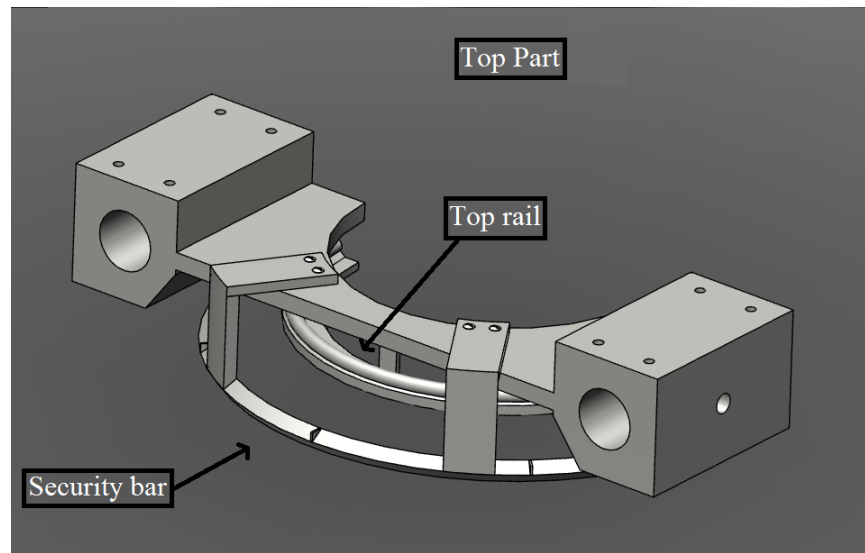


Figure 4.17: Top part of prototype 4: top rail and security bar

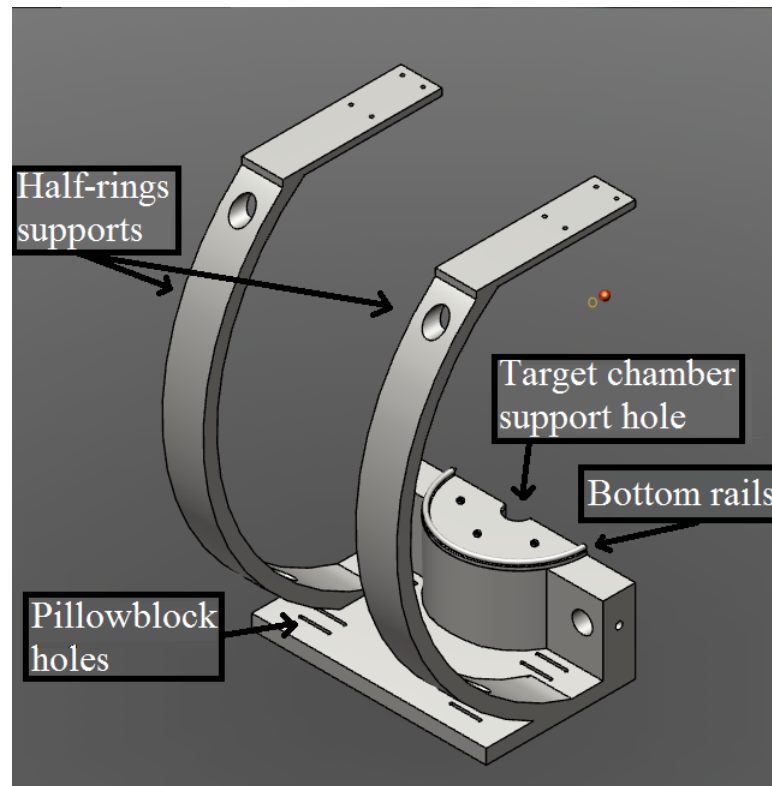


Figure 4.18: Bottom part of prototype 4: bottom rail and half-ring supporters

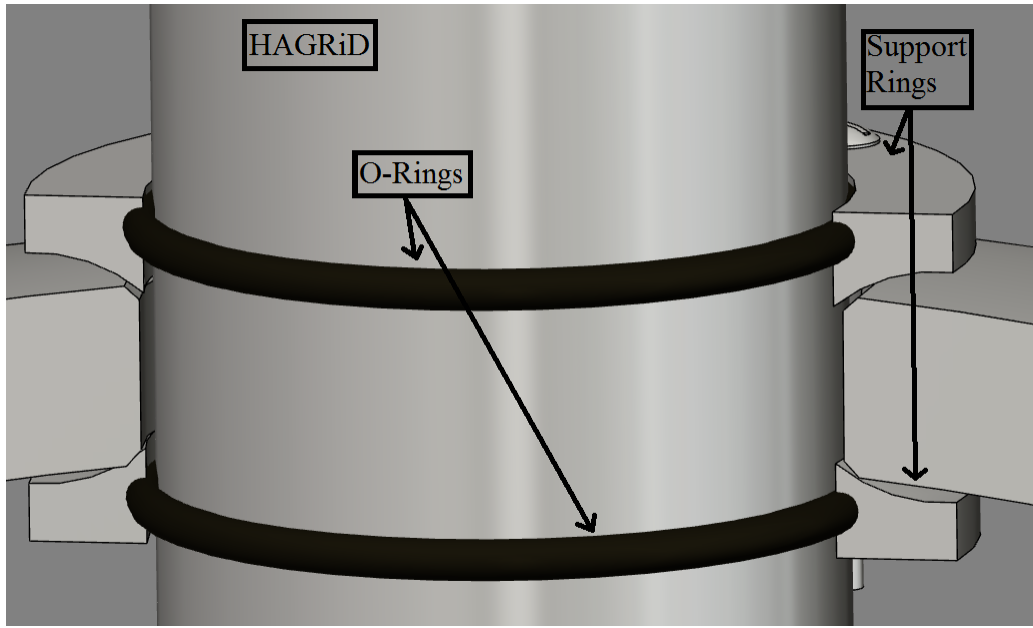


Figure 4.19: Detail of the rings holding the detector with O-rings

The problem presented with the supporting rings on prototype 3 (figure 4.14), where the pressure created by them might damage the detectors, was fixed by adding O-rings (-228). These rubber rings will be between the supporting rings and the detector (see figure 4.19), adding a layer of soft material that will help prevent damage to the detector if too much pressure is applied.

The design for the peel was not altered significantly, only the top and bottom were modified to adjust to the other changes made to the frame (see figure 4.20). The HAGRID detectors, however, were aligned and the angle of each detector was measured to make the data analysis easier. This means that all of the holes positioned in the peels of prototype 3 were repositioned for the peels in prototype 4.

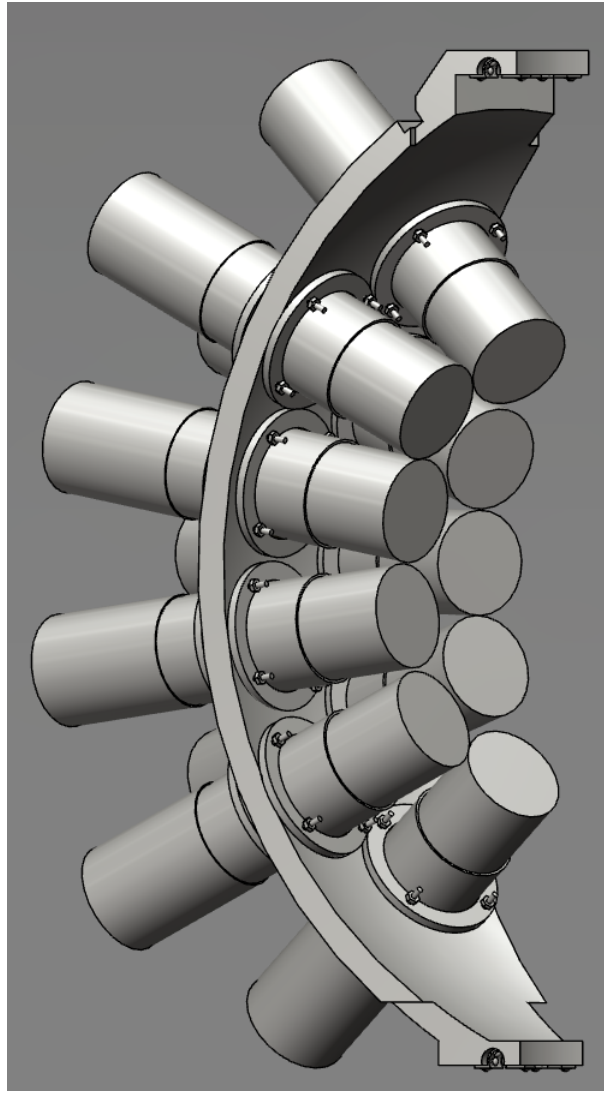


Figure 4.20: Peel design of prototype 4 with HAGRiD detectors

Figure 4.21 shows the whole design of prototype 4 without the HAGRiD detectors while figure 4.22 shows the whole design with the HAGRiD detectors. In this figure we have space for a total of 72 HAGRiD detectors. The only problem with this design is that the peels once mounted on the rails, can not rotate. While a device that would allow the peels to rotate could be designed, it would take a lot of time do the necessary testing so the device would not fail. For these reasons a commercial device is being sought for this purpose.

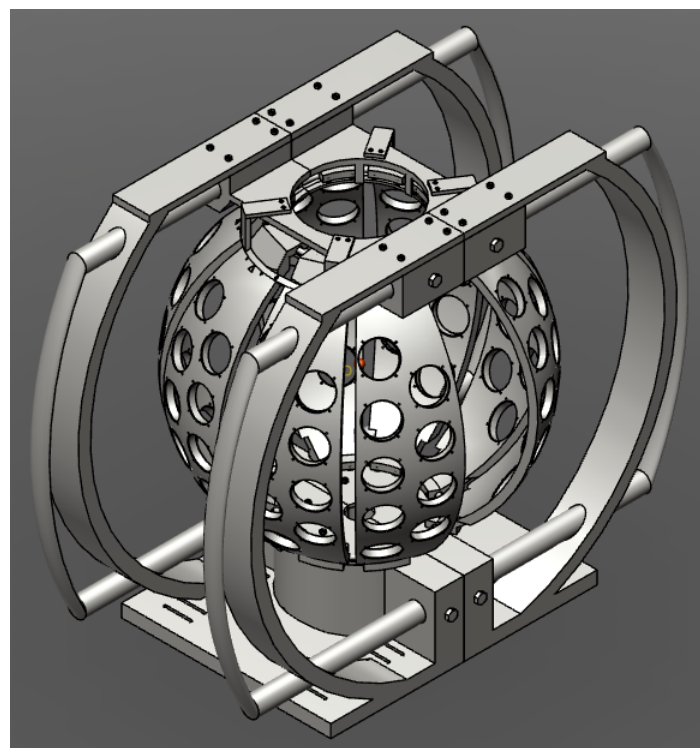


Figure 4.21: Prototype 4 without HAGRID detectors

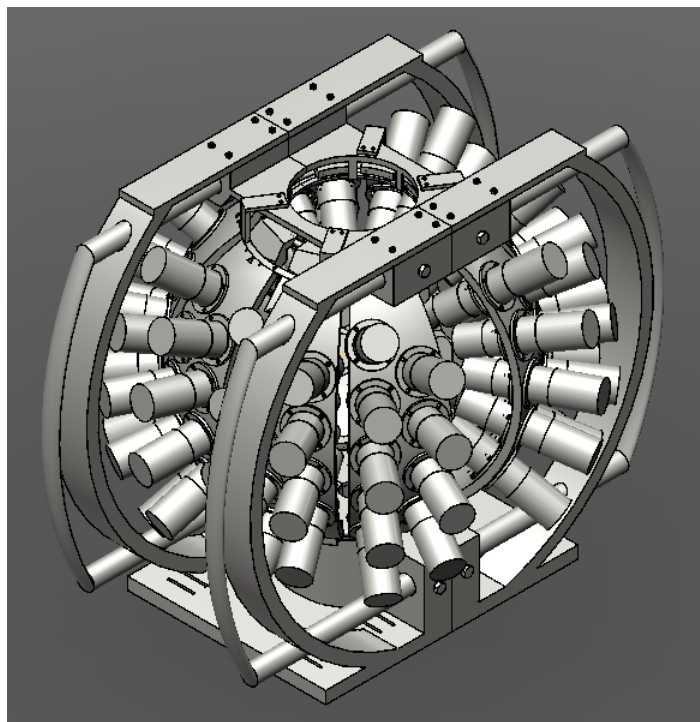


Figure 4.22: Prototype 4 with HAGRID detectors

Chapter 5

Conclusion: Final Design

The frame for HAGRiD is still a work in progress but it is safe to say that Prototype 4 will be the design that will be used for the frame. The HAGRiD frame is expected to be used in different laboratories and with different chambers, for this reason an all-purpose mount was designed. Figure 5.1 shows the mount with the HAGRiD frame which will be mounted on rails to allow the halves to be separated for easy access to the chamber and the chamber's support in the middle.

The HAGRiD mount will also have a support structure on top to allow the placement of the preamplifiers. To connect the HAGRiD frame to the rail in HAGRiD mount, the pillow block from Thomson Industries will be used. Figure 5.2 shows the concept that was used for the final design of the HAGRiD frame and mount, with figure 5.3 showing how the pillow blocks will be positioned on the HAGRiD frame.

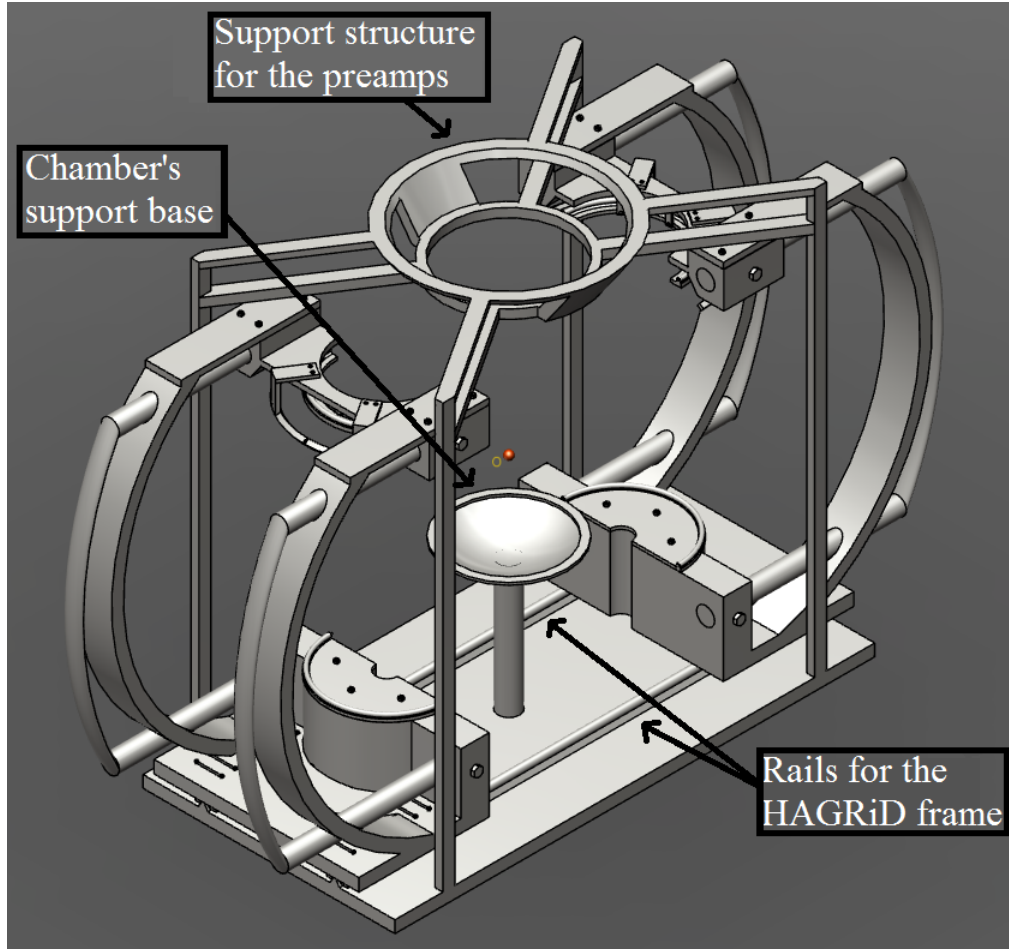


Figure 5.1: The HAGRID frame with the HAGRID mount

The end product is shown in figure 5.4 along with the GODDESS chamber and the peel with HAGRID. The design for the peel might have to be changed, since the peels can not rotate around the target yet and as stated in section 4.3.4, a commercial device is recommended. This design is still a work in progress, so the final design might change, but will likely not be drastically altered.

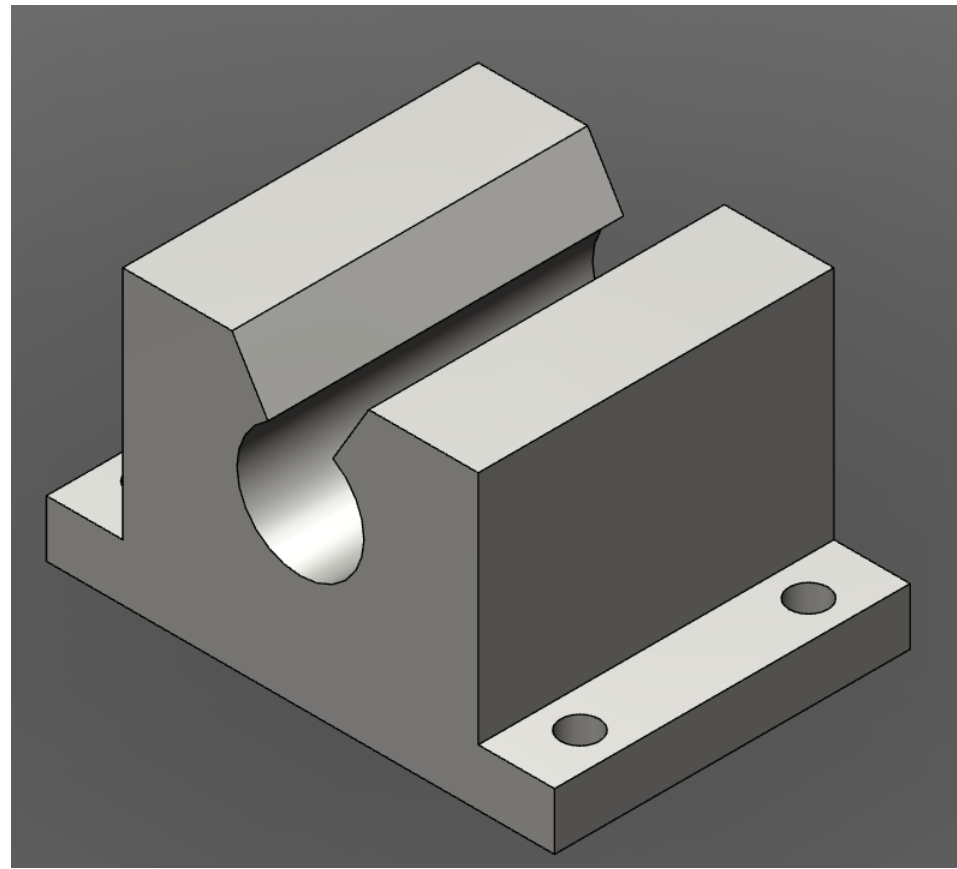


Figure 5.2: The TSPB 10 open from Thomson Industries

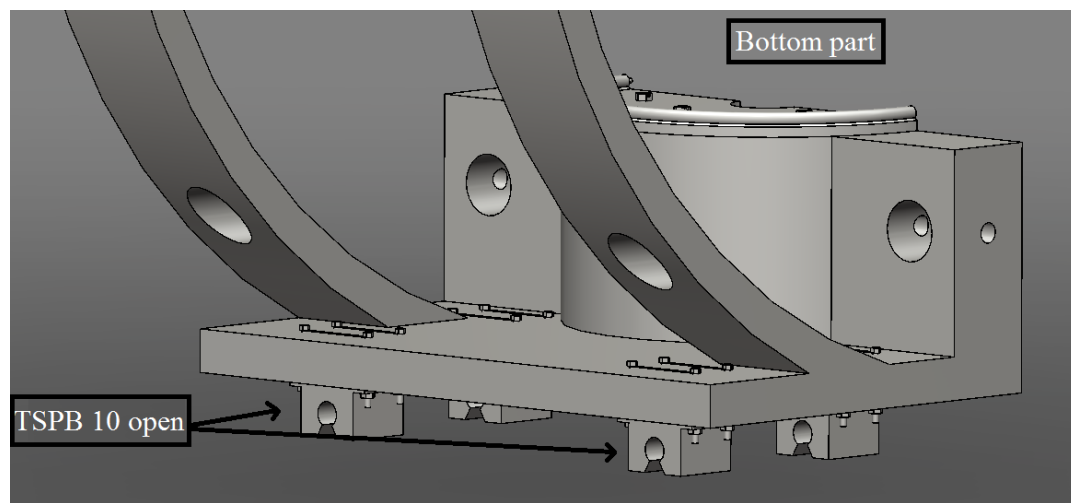


Figure 5.3: Detail of assemble between pillow block and the HAGRiD frame

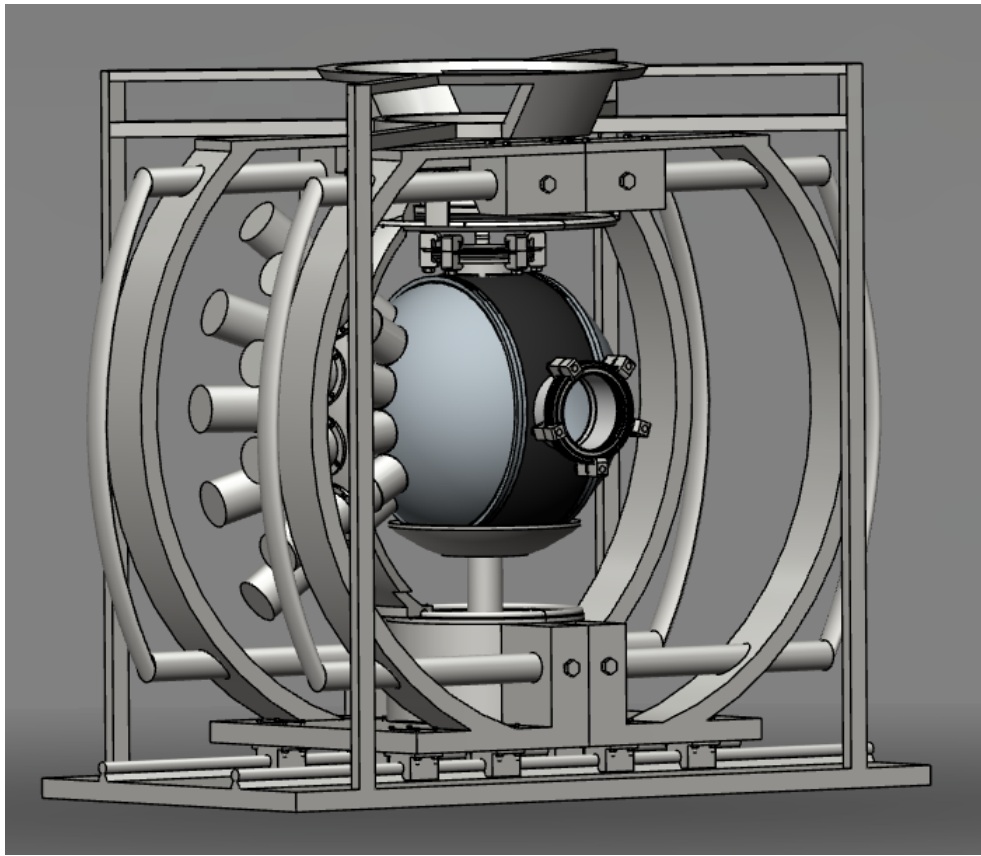


Figure 5.4: Final design for HAGRiD frame and mount with the GODDESS chamber

Bibliography

- [1] D. Lunney, J.M. Pearson, C. Thibault *Recent trends in the determination of nuclear masses* Reviews of modern physics, Volume 3, July 2003.
- [2] Kenneth S. Krane, *Introductory Nuclear Physics*. Jhon Wiley & Sons, 2nd edition, 1955. [viii](#), [ix](#), [3](#), [6](#), [7](#), [8](#), [9](#), [10](#), [11](#), [17](#), [22](#)
- [3] Wapstra, A. H. and Bos, K., "The 1983 atomic-mass evaluation. I. Atomic mass table" Nucl Phys, A 432, 1-54, 1985. [3](#)
- [4] K. L. Jones. *et al. The magic nature of ^{132}Sn explored through the single-particle states of ^{133}Sn .* nature, Vol 465, 2010. [viii](#), [4](#), [18](#), [20](#)
- [5] J.M. Allmond. *et al. Double-Magic Nature of ^{132}Sn and ^{208}Pb through Lifetime and Cross-Section Measurements* Phys. Rev. Lett., PRL 112 2014. [viii](#), [ix](#), [18](#), [19](#), [20](#)
- [6] K. L. Jones. *Transfer reaction experiments with radioactive beams: from halos to the r-process.* Phys. Scr., T152, 2013.
- [7] B. D. Milbrath. *et al. Comparison of LaBr₃:Ce and NaI(Tl) Scintillators for Radio-Isotope Identification Devices* Pacific Northwest National Laboratory, PNNL-15831 2006. [ix](#), [25](#)
- [8] William. R. Leo, *Techniques for Nuclear and Particle Physics Experiments.* Springer-Verlag, 2nd edition, 1994. [23](#)
- [9] Richard A. Dunlap, *The Physics of Nuclei and Particles.* Brooks/Cole, 1st edition, 2004.
- [10] S.D. Pain. *et al.* Nucl. Inst. and Meth. in phys. Res. B 261, 1122, 2007. [26](#)
- [11] A. Ratkiewicz, S.D. Pain, J.A. Cizewski, D.W. Bardayan, J.C. Blackmon, K.A. Chipps, S. Hardy, K.L. Jones, R.L. Kozub, C.J. Lister *et al.* AIP Conference Proceedings, 1525, 487, 2004. [ix](#), [27](#)

- [12] D.W. Clare and D.L. Kepert, *The Optimal Packing of Circles on a Sphere* Journal of Mathematical Chemistry, issue 6 1991. [35](#)
- [13] William Riley, Leroy Sturges and Don Morris, *Mechanics of Materials*. Jhon Wiley & Sons, 6th edition, 2007. [x](#), [55](#), [56](#)

Appendices

Appendix A

Stress and Strain

The intensity of the internal forces that each part of a machine or structure is subject to and the deformation that each part experiences during its intended function, are an important part of every design. Stress and strain always present constraints. The geometry of the body needed to be designed with certain dimensions so that it would not collapse under its own weight or get deformed.

A.1 Stress

Stress is a quantitative measure of a applied force to a stationary body. In order for a body to be effective, it needs to withstand stress, so that it does not rupture or deform excessively. Based on Newton's 3rd law, if a force P is applied to an object, like in figure A.1 (where $a-a$ represents a plane that cuts the body to show the internal force), the system is balanced by an internal force F , normal to the surface, with equal magnitude to P .

Stress can be define by the follow equation:

$$\sigma = F \div A \quad (\text{A.1})$$

Here σ represents applied stress, F is the internal force and A is the cross sectional area of the body.

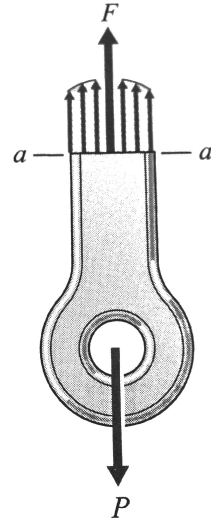


Figure A.1: The free-body diagram of a body. Image modified from [13], p.49.

A.2 Strain

Strain is the relative change in shape or size of a body due to an external applied force, in other words it is the magnitude of a deformation in the same way that Stress is the magnitude of an applied force. There are two types of *Strain*; *Normal strain* (also known as *Axial strain*), denoted with the Greek letter epsilon (ϵ); and *Shearing strain* denoted with the Greek letter gamma (γ) (as shown in Fig. A.2b). To obtain the *strain* of a body, the deformation of the body is needed as shown in Figure A.2 with the Greek letter delta (δ) with the subscript n for Normal strain (a) and s for

Shearing strain (b). The *strain* is equal to the respective deformation divided by the original length of the body L .

$$\epsilon = \delta_n \div L, \quad (\text{A.2a})$$

$$\gamma = \delta_s \div L \quad (\text{A.2b})$$

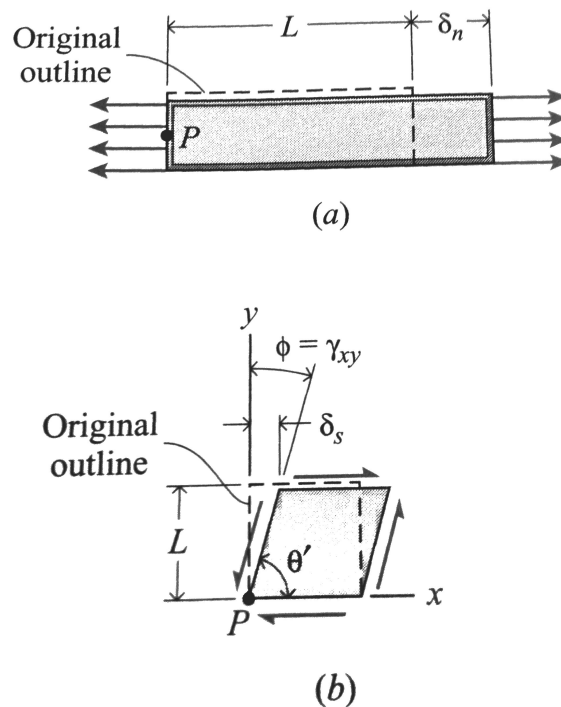


Figure A.2: Diagram of strain. Image modified from [13], p.123.

Auto-CAD Inventor Professional 2014® was used to obtain *Stress/strain* simulations of each design of the frame to ensure that there would be no deformation or rupture.

Figure A.3 shows the stress and strain test performed on the bottom part of prototype 4 (see figure 4.18). In this simulation the two top arrows represent 200 pounds of force, with the bottom arrow representing the direction of gravity.

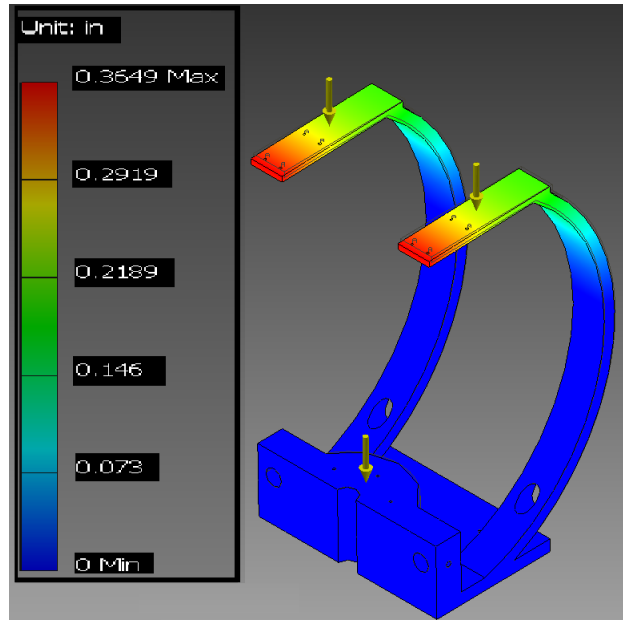


Figure A.3: Stress/strain simulation of the frame in prototype 4.

The figure A.3 (for example) gives important data, in this case it shows that the top parts of the frame (the brighter color area) experience a displacement of .365 inches (max) due to the 200 pound of force, this means that the frame does not suffer any large deformity or rupture and can hold the weight of the detectors and the rest of the frame.

Vita

Santiago was born in Medellin, Colombia on September 9th, 1984. He attended the high school of the University Potifícia Bolivariana, where he graduated in 2001. He moved to United States on December of 2002 and he graduated from Start's Mill High School in May 2004. He started his undergraduate studies on fall of the same year at Gordon State College where he studied physics with a concentration on mechanical engineering. He transferred to the University of West Georgia in fall of 2007. Santiago received his degree of Bachelors of Science in Physics in May of 2010. He got accepted to the University of Tennessee Knoxville (UTK) Physics department where he started studying on fall of 2011. Santiago will receive his Masters degree in Nuclear Physics on December of 2014.